Title

Quantitative Proteomics Reveals Fundamental Regulatory Differences in Oncogenic HRAS and Isocitrate Dehydrogenase (IDH1) Driven Astrocytoma.

Journal

Molecular & cellular proteomics : MCP, 16(1)

ISSN

1535-9476

Authors

Doll, Sophia
Urisman, Anatoly
Oses-Prieto, Juan A
et al.

Publication Date

2017

DOI

10.1074/mcp.m116.063883

Quantitative Proteomics Reveals Fundamental Regulatory Differences in Oncogenic HRAS and Isocitrate Dehydrogenase (IDH1) Driven Astrocytoma*[S]

Sophia Doll‡‖, Anatoly Urisman‡, Juan A. Oses-Prieto‡, David Arnott§, and Alma L. Burlingame‡¶

Glioblastoma multiformes (GBMs) are high-grade astrocytomas and the most common brain malignancies. Primary GBMs are often associated with disturbed RAS signaling, and expression of oncogenic HRAS results in a malignant phenotype in glioma cell lines. Secondary GBMs arise from lower-grade astrocytomas, have slower progression than primary tumors, and contain IDH1 mutations in over 70% of cases. Despite significant amount of accumulating genomic and transcriptomic data, the fundamental mechanistic differences of gliomagenesis in these two types of high-grade astrocytoma remain poorly understood. Only a few studies have attempted to investigate the proteome, phosphorylation signaling, and epigenetic regulation in astrocytoma. In the present study, we applied quantitative phosphoproteomics to identify the main signaling differences between oncogenic HRAS and mutant IDH1-driven glioma cells as models of primary and secondary GBM, respectively. Our analysis confirms the driving roles of the MAPK and PI3K/mTOR signaling pathways in HRAS driven cells and additionally uncovers dysregulation of other signaling pathways. Although a subset of the signaling changes mediated by HRAS could be reversed by a MEK inhibitor, dual inhibition of MEK and PI3K resulted in more complete reversal of the phosphorylation patterns produced by HRAS expression. In contrast, cells expressing mutant IDH1 did not show significant activation of MAPK or PI3K/mTOR pathways. Instead, global downregulation of protein expression was observed. Targeted proteomic analysis of histone modifications identified significant histone methylation, acetylation, and butyrylation changes in the mutant IDH1 expressing cells, consistent with a global transcriptional repressive state. Our findings offer novel mechanistic insight linking mutant IDH1 associated inhibition of histone demethylases with specific histone modification changes to produce global transcriptional repression in secondary glioblastoma. Our proteomic datasets are available for download and provide a comprehensive catalogue of alterations in protein abundance, phosphorylation, and histone modifications in oncogenic HRAS and IDH1 driven astrocytoma cells beyond the transcriptomic level. ***Molecular & Cellular Proteomics 16: 10.1074/mcp.M116.063883, 39–56, 2017.***

Gliomas are the most common human brain tumors with ~250,000 cases per year worldwide (1). Gliomas arise from glial cells, which are non-neuronal cells that provide support and protection for neurons. Astrocytomas are the most common form of glioma (2) and are histologically categorized into four grades (I–IV), of which grade III (anaplastic astrocytoma), and grade IV (glioblastoma multiforme (GBM)[1]), are malignant (3). GBMs are among the deadliest human cancers, and despite the use of aggressive multimodality therapy combining surgery, radiotherapy, and chemotherapy, less than 5% of patients survive longer than 5 years after diagnosis (4). Although most GBMs (90%) develop *de novo* (primary glioblastoma) and typically have rapid progression, some (10%) progress more slowly after initially presenting as low-grade gliomas (secondary glioblastoma) (supplemental Fig. S1) (5).

Most common alterations in primary glioblastomas include telomerase reactivation, p53 and pRB pathway deactivation, PTEN loss, and EGFR amplification leading to RAS signaling activation (6). RAS network alterations (other than by mutation, which is rare in gliomas) are commonly observed in malignant astrocytomas (7–10). Importantly, overexpression of HRAS in normal human astrocytes (NHAs) results in the formation of intracranial tumors strongly resembling human

From the ‡Department of Pharmaceutical Chemistry, University of California, San Francisco, 94158–2517 California; §Department of Protein Chemistry, Genentech Inc, South San Francisco, 94158–2517 California

Received September 12, 2016, and in revised form, November 4, 2016

Published, MCP Papers in Press, November 10, 2016, DOI 10.1074/mcp.M116.063883

Author contributions: S.D. designed research; S.D. performed research; S.D. analyzed data; S.D. wrote the paper; A.U. helped with the biological interpretation; J.A.O. mass spectrometry support; D.A. supervised the histone ptm analysis; A.L.B. supervised the project.

[1] The abbreviations used are: GBM, glioblastoma multiforme; NHA, normal human astrocytes; PTM, post-translational modification; hTERT, human telomerase reverse transcriptase.

grade III anaplastic astrocytoma after injection into mice. In contrast, activation of AKT or EGFR does not trigger this transformation (7). RAS remains difficult to target and several small molecule inhibitors targeting downstream nodes of the RAS regulated core axis have been developed for potential cancer treatment. For example, cobimetinib (Genentech Inc., South San Francisco, CA) and pictilisib (Genentech Inc.) are both highly selective and potent inhibitors of MEK1/2 and PI3K, respectively (11, 12). MEK or PI3K inhibitors as single agents in GBM therapy, however, lack of efficacy and require the development of more effective therapies (13, 14).

Over 70% of secondary glioblastomas harbor isocitrate dehydrogenase 1 (IDH1) mutations, involving Arg132 in nearly all cases, whereas primary glioblastoma rarely show IDH mutations (15–17). It has been shown that IDH1 Arg132 mutation suppresses the biochemical ability of IDH1 to convert isocitrate into α-Ketoglutarate (α-KG) by further converting α-KG into 2-hydroxyglutarate (2-HG) (18). As a result, the oncometabolite 2-HG accumulates at high levels in IDH1 mutant tumors (up to 100-fold of normal) and inhibits α-KG-dependent histone and DNA demethylases, affecting epigenetic regulation and associated gene expression (supplemental Fig. S2) (19, 20). Although 60 other human α-KG-dependent dioxygenases exist (21), α-KG-dependent histone demethylases are the most sensitive to 2-HG-mediated inhibition (20). Other epigenetic alterations induced by mutant IDH1 include the CpG island methylator phenotype (CIMP), characterized by increased global DNA methylation (22). However, more detailed mechanisms of tumorigenesis produced by accumulation of 2-HG and CIMP in IDH1-mutant gliomas, including specific alterations in signaling pathways and key epigenetic factors responsible for transformation and progression, remain largely unknown.

To uncover possible mechanisms driving the cellular and molecular transformation of primary and secondary glioblastoma, we investigated changes of protein abundance, phosphorylation, and histone post-translational modifications (PTMs) in an *in vitro* model. Direct analysis of proteins and PTMs provides an important advantage over genomic and transcriptomic approaches, because mRNA expression often does not correlate with protein expression and cannot predict functional state of proteins determined by PTMs (23, 24). Only a few studies have attempted to investigate the alterations in phosphorylation within signaling networks in human gliomas (25–27), but none have addressed the potential involvement of an altered histone code by targeted quantitative mass spectrometry (MS). MS-based proteomics provides a platform for in-depth identification and quantification of thousands of proteins and their PTMs, including histone PTMs, and allows the quantitation of perturbed signaling networks (28).

To study these mechanisms *in vitro*, we chose a previously developed cellular model (7, 29). This system consists of NHAs, which are immortalized by the reactivation of telomerase activity via the expression of human telomerase reverse transcriptase (hTERT) and the introduction of virally-encoded E6 and E7 to inhibit the transcription of p53 and pRb, respectively. NHA E6/E7 hTERT (control-NHA) are further transformed into tumorigenic astrocytoma cells by either overexpressing oncogenic H-Ras V12 (RAS-NHA) or introducing mutant IDH1 (IDH1mut-NHA), mimicking primary and secondary high-grade astrocytoma, respectively.

In this work we applied a quantitative MS-based strategy to characterize the proteomic and phosphoproteomic changes in HRAS and mutant IDH1 driven glioma cells. We report the driving roles of the MEK and PI3K signaling pathways in RAS-NHA cells, and describe previously unknown alterations in other pathways. Furthermore, we show that simultaneous MEK and PI3K inhibition reverses many but not all signaling changes driven by oncogenic HRAS in RAS-NHA cells**.** Additionally, we provide a quantitative view of major effects on histone PTM occupancies resulting from the overproduction of the oncometabolite 2-HG and its inhibition of chromatin remodeling enzymes in IDH1mut-NHA cells.

EXPERIMENTAL PROCEDURES

Cell Culture—Immortalized NHAs were a gift from R. O. Pieper (University of California San Francisco, CA). The creation of NHA expressing E6/E7 and hTERT (control-NHA), NHA expressing E6/E7, hTERT, and IDH1mutant (IDH1mut-NHA), and NHA expressing E6/E7, hTERT, and H-Ras V12 (RAS-NHA) has been described previously (7, 30). IDH1mut- and RAS-NHA cells were cultivated in stable isotope labeling by amino acids in cell culture (SILAC) DMEM-H21 medium (Thermo Fisher Scientific, Waltham, MA) supplemented with 10% dialyzed FBS and 1% Penicillin Streptomycin containing heavy $^{13}C_6{}^{15}N_2$-lysine and $^{13}C_6{}^{15}N_4$-arginine (R10K8) or medium $^{2}H_4$-lysine and $^{13}C_6$ arginine (R6K4) (Cambridge Isotope Laboratories, Andover, MA), respectively. Control-NHA cells were grown in SILAC DMEM-H21 medium supplemented with light lysine and arginine (R0K0). All cell lines were maintained at 37 °C and 5% CO_2 and collected after a minimum of 5 passages.

Immunoblotting—To prepare the lysates for immunoblot assays, cells were lysed in RIPA buffer (Thermo Fisher Scientific) supplemented with 1% phosphatase and protease inhibitors. Samples were rocked at 4 °C for 30 min and cleared by centrifugation at 10,000 rpm for 10 min at 4 °C. Protein levels were measured using the Pierce BCA protein assay (Thermo Fisher Scientific) by fluorescence spectrometry. Equal amount of protein extracts were incubated at 70 °C in LDS sample buffer and reducing agent (Invitrogen, Carlsbad, CA) for 10 min before being separated by SDS-polyacrylamide gel electrophoresis (NuPAGE, Invitrogen) and transferred to a nitrocellulose membrane. After blocking for 1 h at room temperature with bovin serum albumin, membranes were incubated with primary antibodies overnight at 4 °C. Anti-nestin (NES) antibody was obtained from Santa Cruz Biotechnology. Specific antigen-antibody interaction was detected with anti-mouse secondary antibodies labeled with horseradish peroxidase (HRP). Signal was revealed by SuperSignal West Pico Chemiluminescent HRP substrate (Thermo Fisher Scientific).

MEK and PI3K Inhibition—We treated heavy SILAC-labeled RAS-NHA cells with 2 μM of cobimetinib (GDC-0973, Genentech Inc.) and unlabeled RAS-NHA cells with DMSO for 4 h. Dual MEK and PI3K inhibition was carried out by the addition of 2 μM GDC-0973 and 5 μM pictilisib (GDC-0941, Genentech Inc.). After 4 h, cells were collected and stored at −80 °C. GDC-0973 and GDC-0941 drug concentrations were selected based on previously described conditions (31).

Sample Preparation and Titanium Dioxide (TiO_2) Phosphopeptide Enrichment—After full incorporation of SILAC labels, cell pellets were collected and stored at −80 °C. Cell pellets were lysed in 8 M urea, 20 mM HEPES buffer by sonication and clarified by centrifugation at 16000 × *g* for 10 min. Protein content was measured using Pierce BCA protein assay (Thermo Fisher Scientific) according to the manufacturer's protocol. Heavy and medium SILAC-labeled samples were combined with the unlabeled sample at 1:1:1 final protein content ratio. Proteins were reduced with dithiothreitol and alkylated with iodoacetamide prior to overnight tryptic in-solution digestion at 37 °C. Tryptic peptides were further desalted with Sep-Pak C18 cartridges (Waters Corporation, Milford, MA). Peptides were enriched for phosphopeptides with an in-house packed TiO_2 column using an AKTA Purifier HPLC system (GE Healthcare, Chicago, IL) as described previously (32). Both, phosphopeptide and flowthrough (non-phosphorylated peptides) fractions were further fractionated by off-line high-pH reversed phase chromatography into 20 fractions as previously described (32). The fractions were desalted with Zip Tip C18 pipette tips (Millipore Corporation, Billerica, MA) before liquid chromatography tandem mass spectrometry (LC-MS/MS) analysis. This experiment was repeated in three biological replicates.

To assess the SILAC labeling efficiency, about 200 μg of proteins of heavy RAS-NHA and medium IDH1mut-NHA SILAC-labeled samples were separately reduced, alkylated, and digested before LC-MS/MS analysis as described above.

LC-MS/MS Analysis—Nanoflow LC-MS/MS analysis of tryptic peptides was conducted on an LTQ-Orbitrap Velos (Thermo Fisher Scientific) fitted with an EASY-Spray PepMap® RSLC C18, 3 μm, 100 Å, 75 μm × 15 cm column (Thermo Fisher Scientific). About 0.4 μg of desalted peptides were loaded and eluted over the course of 57 min from 2–27% solvent B (100% acetonitrile, 0.1% formic acid) and stepped up to 50% in 2 min. The mass spectrometer was operated in "top-6" data-dependent mode, collecting MS spectra in the Orbitrap mass analyzer (60000 resolution, 350–1500 m/z range) with an automatic gain control (AGC) target of 2E6 and a maximum ion injection time of 250 ms. Following higher-energy collisional dissociation (HCD), MS/MS spectra were collected in the Orbitrap (7500 resolution, 350–1500 *m/z* range) with an AGC target of 9E4 and a maximum ion injection time of 500 ms. Label free analysis was performed on an Orbitrap Fusion mass spectrometer in a "top-10" data-dependent mode, collecting MS spectra in the Orbitrap (120,000 resolution, 375–1600 *m/z* scan range) with an AGC target of 2E5 and a maximum ion injection time of 50 ms. After HCD fragmentation, MS/MS spectra were collected in the Orbitrap (30,000 resolution, 350–1400 *m/z* scan range) with an AGC target of 5E4 and a maximum injection time of 60 ms. Desalted peptides were loaded on an EASY-Spray PepMap® RSLC C18, 2 μm, 100 Å, 75 μm × 15 cm column (Thermo Fisher Scientific) and eluted over the course of 85 min with an acetonitrile gradient from 2–25% solvent B (98% acetonitrile, 0.1% formic acid) and stepped up to 40% in 2 min.

Experimental Design and Statistical Rationale—For the characterization of the proteomic and phosphoproteomic changes in HRAS and mutant IDH1 driven glioma cells, we applied a SILAC quantitative MS-based strategy. Biological triplicates of each triple-SILAC experiment provided *p* values for the statistical analyses. An additional label free quantification was measured to validate the proteomic changes observed in IDH1mut-NHA cells compared with control cells. Two technical replicates were measured for the analysis of histone PTM changes of IDH1mut- IDH1wt-, and control-NHA cells.

Data Analysis—Tandem mass spectra were searched against the UniProt_2015_07 human database (containing 68561 entries) using MaxQuant version 1.5.2.8 with a 1% false discovery rate (FDR) at the phosphosite, peptide, and protein level. Default settings with the following changes were applied: "phospho (STY)" were selected as variable modifications for phosphopeptide searches, "re-quantify" and "match between runs" were enabled, and a minimum ratio count of 1 was selected, meaning that at least one labeled peptide triplet needs to be quantified to report a SILAC ratio. Carbamidomethylation of cysteine was selected as fixed modification and N-terminal protein acetylation and methionine oxidation as variable modifications and a maximum of two missed cleavages was selected with trypsin as protease. The mass tolerance for precursor ions and fragment ions were 20 ppm. Bioinformatics analysis was performed with Perseus version 1.5.1.6, Microsoft Excel, and R statistical software. Heavy/light and medium/light log2 ratios were calculated for each detected protein and normalized by median-centering (*i.e.* setting the median log2 ratio equal to zero). Average log2 ratios from the biological repeats and the corresponding *p* values were visualized with volcano plots. *p* values were calculated based on a *t* test and a *p* value of $<$ 0.05 and fold change of $>$ 2 (log2 $>$ 1) were chosen as the significance cutoff based on the distributions observed in volcano plots. All raw data, search parameters, and results are available on ProteomeXchange via the PRIDE database (PXD004945). We provide further information about all identified phosphopeptides in supplemental Tables S1–S3 and the annotated spectra can be visualized using the ProteinProspector MS-viewer with the following search keys: rqb1zvxx60 (triple SILAC experiment, supplemental Table S1), t334dbbxng (MEK inhibition experiment, supplemental Table S2), and w8fxjv0hoj (dual MEK and PI3K inhibition experiment, supplemental Table S3).

Gene Ontology, Molecular Signature Database (MSigDB) and Principal Component Analysis (PCA) Analysis—To identify enriched biological processes terms within our data set we used DAVID bioinformatics functional annotation tool (http://david.abcc.ncifcrf.gov/) (33). The significance of fold enrichment was calculated using a Benjamini-Hochberg adjusted *p* value of $\leq$ 0.01. Gene set enrichment analysis (GSEA) was performed using gene set collections "h," "c2," "c3," "c4," "c5," and "c6" from the MSigDB (34). We estimated the significance of fold enrichments for each gene set by hypergeometric testing in R. PCA was performed on the processed data as described previously (35).

Histone Purification and Mass Spectrometry Analysis by Parallel Reaction Monitoring (PRM)—H2A, H2B, H3, and H4 histones were purified with a histone purification kit (Active Motif, Carlsbad, CA) according to the manufacturer's protocol. Histone concentrations were measured using Direct Detect Infrared Spectrometer (Millipore). In total, 4 μg of unlabeled histones (extracted from IDH1mut-, IDH1wt-, and RAS-NHA cells) and heavy amino acid-labeled histones (extracted from PC9 cells, used as a common standard) were mixed in a 1:1 ratio. Histone digestion and MS analysis were performed as previously described (36). Briefly, histones were propionylated using deuterated propionic anhydride; the reaction was quenched by hydroxylamine followed by tryptic digestion overnight and phenyl-isocyanate (PIC) labeling. Histone peptides were then analyzed by capillary reversed phase ultra high-pressure liquid chromatography-electrospray ionization tandem MS on an Orbitrap Fusion mass spectrometer as described previously (37). Targeted product ion spectra were acquired by PRM based on a targeted inclusion list containing 72 transitions covering 100 peptide combinations and 71 distinct histone PTMs for histones H3 and H4. Data were further processed with Skyline (38) and the relative abundance of histone PTMs across the samples was normalized using the heavy SILAC-labeled internal standard (PC9 cells). Experiments were repeated twice (technical replicates) and a log2 ratio cutoff of $\geq$ 0.2 was used to define significant changes.

RESULTS AND DISCUSSION

I) Quantitation of Proteomic and Phosphoproteomic Changes by SILAC-MS in RAS or Mutant IDH1 Driven Glioma Cells—To compare signaling alterations in RAS or mutant IDH1 driven

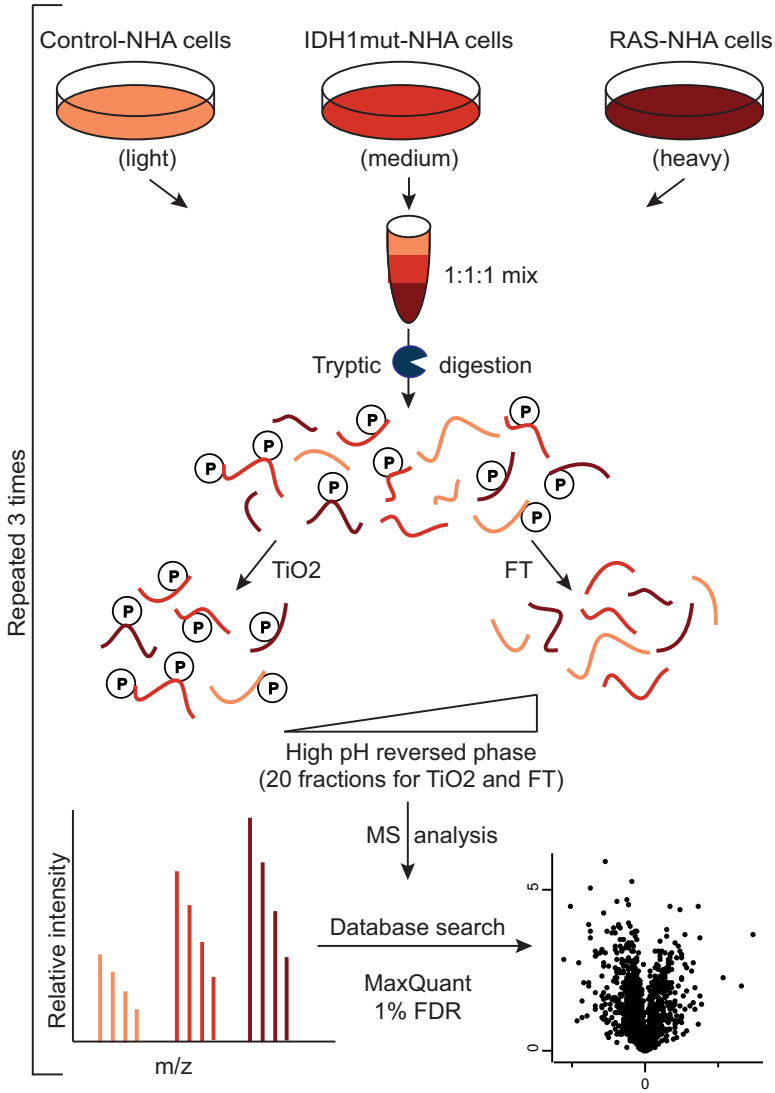

FIG. 1. **Experimental design.** IDH1mut-NHA and RAS-NHA cells were medium and heavy SILAC-labeled, respectively. Control-NHA cells remained unlabeled. Protein lysates were mixed in a 1:1:1 ratio, enzymatically digested, enriched for phosphopeptides by TiO2, and both phosphopeptides and the flow through (FT) were fractionated by high-pH reversed phase chromatography into 20 fractions before analysis by LC-MS/MS. Data were processed using MaxQuant software at 1% FDR.

astrocytoma cell lines we determined proteome-wide phosphorylation and protein abundance changes in immortalized NHA cells in response to overexpression of HRAS or mutant IDH1 using SILAC based MS (39) (Fig. 1*A*). After full incorporation of SILAC labels as assessed by MS (98 and 96% labeling efficiency for RAS-NHA and IDH1mut-NHA cells, respectively (supplemental Table S4)), the phosphorylation and protein abundance changes of these two cell lines were compared with control-NHA cells. Overall, we identified 6942 phosphorylation sites with a 1% FDR at the protein, peptide, and phosphorylation site level. Among these, 4976 phosphorylation sites were mapped with high confidence (localization probability $\geq$ 0.75 (28)) (supplemental Table S5). A total of 2817 of these phosphosites were detected and quantified in at least two of the three biological replicates, and 1402 sites were detected in all three replicates and all three cell types (Fig. 2*A*). The majority (77%) of the detected phosphopeptides were singly phosphorylated, whereas 19% were doubly and 4% triply phosphorylated. A comparison of relative phosphopeptide abundances (ratios to the control-NHA cells) between biological replicates showed high reproducibility, with an average Pearson correlation factor R of 0.77 (supplemental Figs. S3*A* and S4).

We detected a total of 4034 proteins at 1% FDR, of which 2800 proteins were identified in at least two biological replicates, and 1764 proteins were detected in all three biological replicates (Fig. 2*B*). Measured relative protein abundances in the biological replicates showed high degree of reproducibility with an average Pearson correlation factor R of 0.76 (supplemental Fig. S3*B*). MS validated the over-expression of HRAS

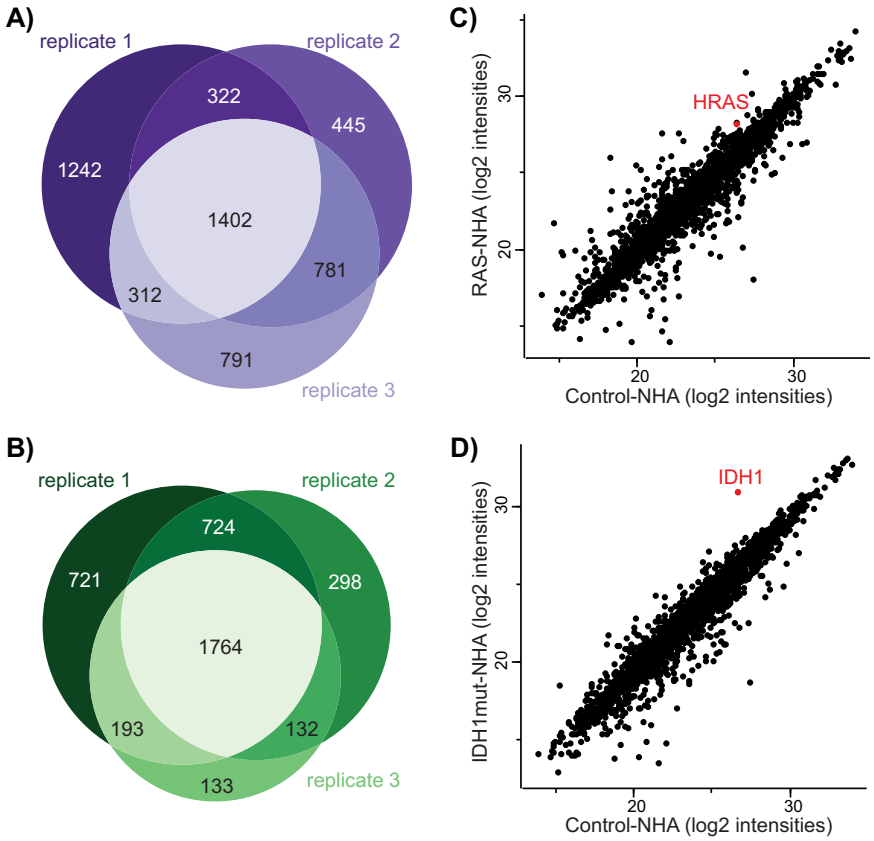

FIG. 2. **Detected proteomes and phosphoproteomes in three biological replicates.** The Venn diagrams indicate the number of (*A*) phosphosites (localization probability ≥ 0.75) and (*B*) proteins identified in each biological replicate. Scatterplots illustrate the comparison of protein intensities (log2) in (*C*) RAS-NHA cells compared with control-NHA cells and (*D*) IDH1mut-NHA cells compared with control-NHA cells in one of three biological replicates.

at the protein level in RAS-NHA cells (Fig. 2*C*). Although previous studies confirmed the presence of the mutant form of IDH1 in IDH1mut-NHA by Western blot (29), we also observed significant over-expression of IDH1 at the protein level (Fig. 2*D*).

II) Characterization of the Phosphoproteome in RAS-NHA Cells—In order to detect signaling network alterations mediated by oncogenic HRAS in glioma, we quantitatively compared phosphorylation changes of RAS-NHA to those of NHA cells as the control. For all comparisons, we used a 2-fold change (log2 ≥ 1) and *p* value of <0.05 cutoff to define significant up or downregulation. Overall, 18.6% of all identified phosphosites in RAS-NHA cells displayed significant changes in regulation (Fig. 3*D*). We found that 278 phosphorylation sites corresponding to 154 proteins showed upregulation, whereas 245 phosphorylation sites, mapping to 160 proteins, displayed downregulation (supplemental Table S6). In total, 672 phosphorylated proteins were also detected in the protein abundance measurements, allowing normalization of phosphorylation changes by the respective protein expression to identify instances of abundance-independent changes in phosphorylation (supplemental Table S7).

A) Affected Pathways Downstream of RAS—*Overexpression of HRAS Triggers Activation of the MAPK and PI3K Pathways*—To identify the biological processes and pathways that are associated with altered phosphorylation after HRAS overexpression, we performed GSEA using MSigDB database of annotated gene sets (34). We found that upregulated phosphoproteins in RAS-NHA cells were significantly enriched for the MAPK ($p = 0.0005$), PI3K ($p = 0.009$), and MTOR ($p = 2e^{-6}$) pathways (Fig. 3*A*). Furthermore, sequences surrounding the regulated phosphosites showed a significant enrichment of canonical MAPK and PI3K substrate recognition motifs (Fig. 3*B*).

MAPK Pathway—Examining the correlation between phosphorylation and protein abundance revealed that a subset of upregulated phosphosites, including MAP2K2, MAPK1, and MAPK3 showed abundance independent upregulation (Fig. 3*C*). Phosphosites of MAPK1 (pT185 and pY187) are known MAP2K1/2 target sites (40) and displayed 3.4- and 6.5-fold abundance independent upregulation in our experiments, respectively. The dual phosphorylation of these two sites is known to promote the kinase activity of MAPK1 and is required for maximal activation (41). Similarly, phosphorylation of MAPK3 on pY204, which is another target site of MAP2K1/2 (42), revealed 6-fold higher abundance-independ-

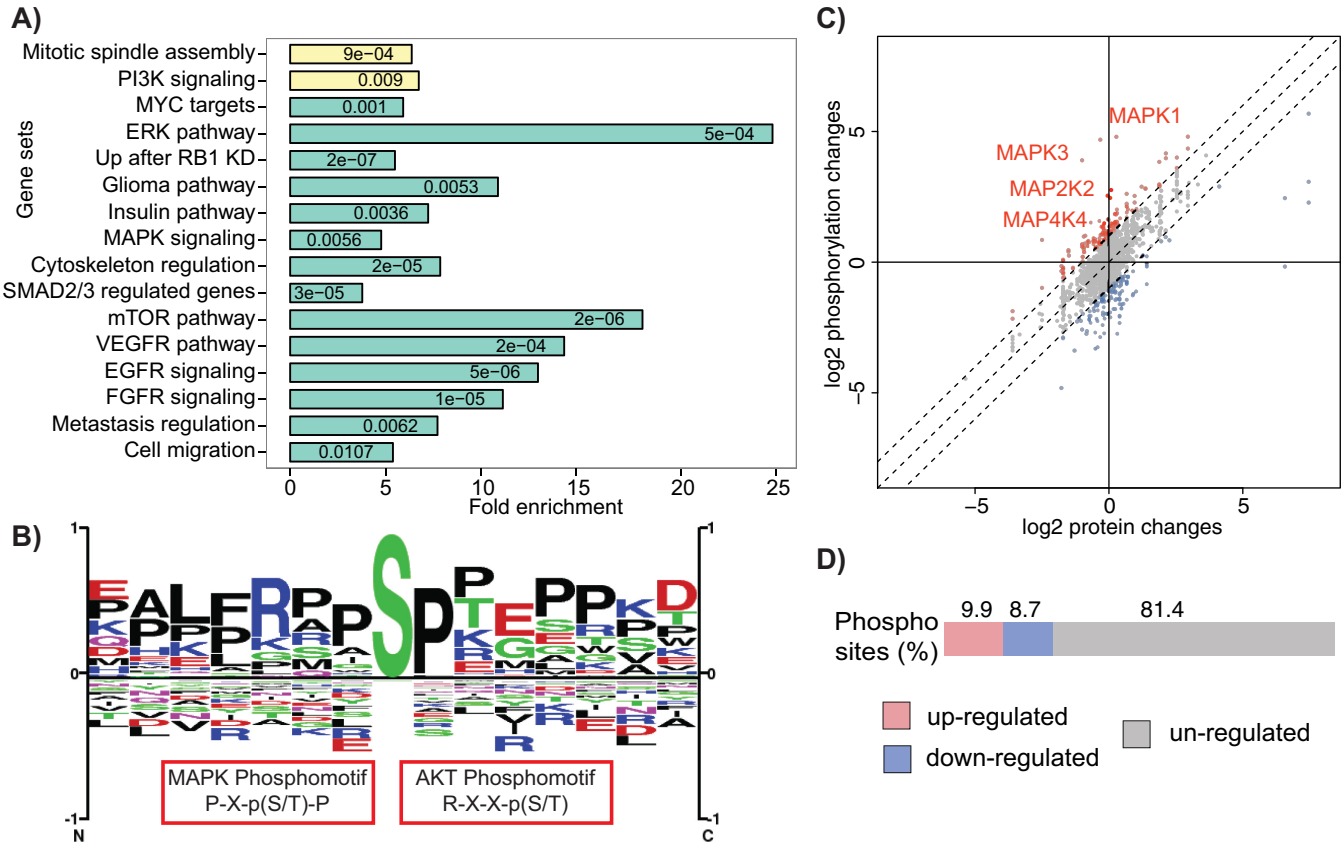

FIG. 3. **MAPK and PI3K signaling pathways are significantly upregulated in RAS-NHA cells.** Upregulated phosphosites are significantly enriched for (*A*) MAPK and PI3K pathways members based on GSEA analysis (*p* values are indicated for each gene set) and (*B*) for MAPK and PI3K phosphorylation motifs. *C*, A subset of at least 2-fold regulated phosphosites show abundance-independent changes in all 3 biological replicates. *D*, Proportion of regulated phosphosites.

ent upregulation (Fig. 4*A* and 4*B*). In addition to perturbed phosphorylation we found multiple changes at the protein abundance level that are consistent with activation of the MAPK pathway. For example, Sprouty protein 4 (SPRY4), whose expression is induced by the MAPK pathway (43, 44), showed a 10-fold upregulation at the protein level.

PI3K Members—We also found that several key members of the PI3K pathway showed regulation at the phosphorylation level, including AKT1S1, RPTOR, and RICTOR (Fig. 4*A* and 4*B*). For example, AKT1S1 phosphosites pT246 and pS212 displayed 3.1-fold and 1.9-fold abundance-independent upregulation, respectively. Both phosphosites have been described as activating and are target sites of AKT1 and MTOR, respectively (45, 46). Phosphorylation of AKT1S1 on residue pT246 promotes activation of the mTORC1. Similarly, phosphorylation of RPTOR on pS863 displayed a 2.6-fold upregulation; this site is also known to indicate mTORC1 activation (47). Activation of mTORC1 leads to the stimulation of its downstream targets including RPS6KB1 and subsequent activation of EIF4B, which triggers transcription of multiple proteins involved in cell proliferation and survival (48). Phosphorylation level of EIF4B (pS93) was identified in one of the three biological replicates and showed 2.2-fold abundance independent upregulation compared with control cells. In contrast, other phosphosites on EIF4B, including pS238 and pS406, did not show significant changes. Interestingly, another member of the EIF family, EIF4E, showed a 2.5-fold or higher increase of phosphorylation on multiple sites in the C-terminal tail, including pT205, pS207, and pS209. The phosphorylation of EIF4E on pS209, known to be mediated by the EIF4G-associated kinases MNK1 and MNK2, promotes cap-dependent translation (49, 50). MNK1/2 are protein-serine/threonine kinases that are activated by MAPK, and inhibition of these two kinases results in decreased glioma formation in mice (51). Notably, pT205 and pS207 phosphosites on EIF4E have not been functionally characterized. Their significant upregulation points to a possible role in regulating the function of EIF4E.

Other regulated proteins in PI3K pathway in RAS-NHA cells included Niban (FAM129A). FAM129A regulates the phosphorylation of multiple proteins involved in translation regulation, including EIF2A, EIF4EBP1 and RPS6KB1. Consistent with overexpression of FAM129A in multiple cancer types (52–54), we observed a 2-fold upregulation of its abundance in RAS-NHA cells. Additionally, we detected a 2-fold upregulation of phosphorylation at pS602. This site is a known substrate of

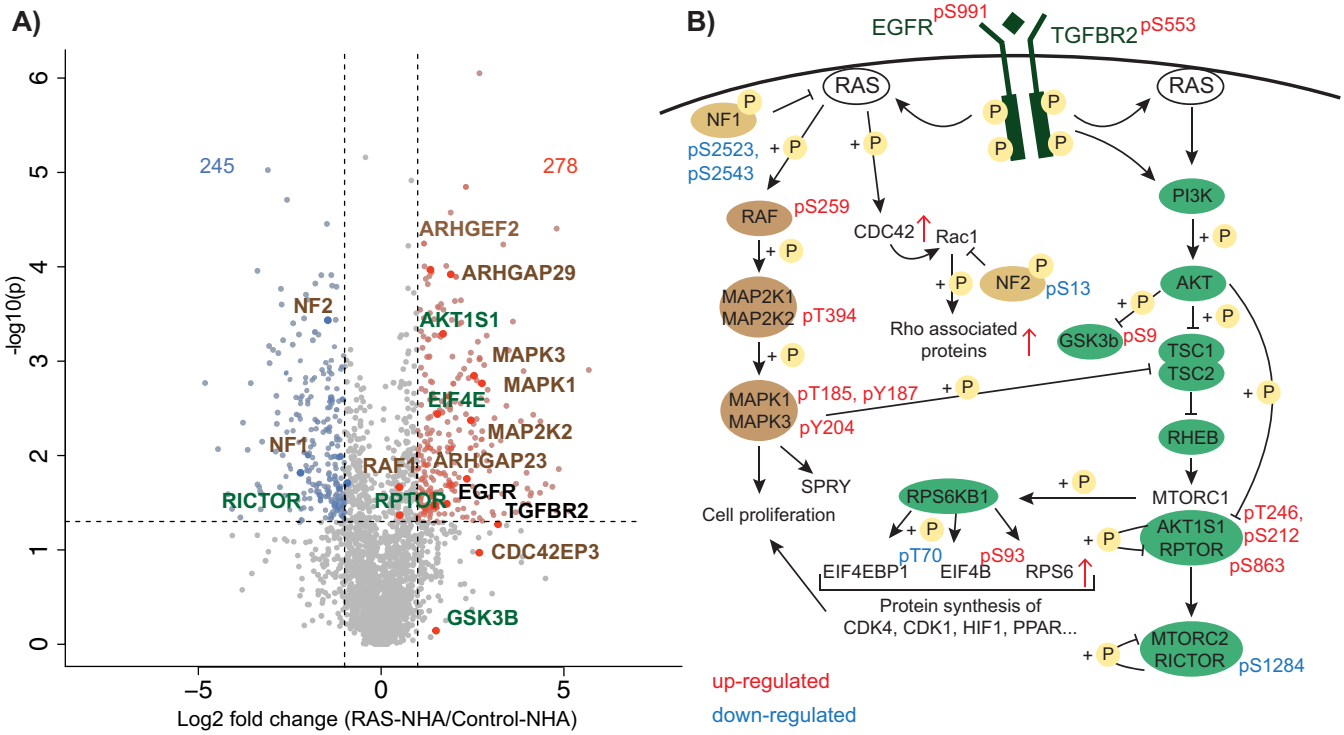

FIG. 4. **Phosphorylation sites involved in the MAPK and PI3K signaling pathways are significantly dysregulated in RAS-NHA cells.** *A*, The volcano plot illustrates the phosphorylation fold changes in RAS-NHA cells compared with control-NHA cells (*x* axis) and the corresponding *p* values reflecting the significance in biological replicates (*y* axis). The MAPK and PI3K are highlighted in *brown* and *green*, respectively. Receptor tyrosine kinases are highlighted in *black*. *B*, Schematic representation of the MAPK (*brown*) and PI3K (*green*) pathways and associated regulated phosphosites.

AKT1. Phosphorylation of FAM129A promotes the degradation of p53 (55), which in our system is consistent with suppression of apoptosis by oncogenic HRAS. We also detected another upregulated (3.7-fold) phosphosite of FAM129A at pS646. The functional role of this phosphosite, however, is unknown. Niban-like protein 1 (FAM129B) also showed significant upregulation of multiple phosphosites (pS641, pS646, pS665, pS681, pS692, pS696) in RAS-NHA cells. FAM129B plays a critical role in cancer cell invasion, primarily by inhibiting caspase-mediated apoptosis (56). Although MAPK regulated signaling has been shown to mediate phosphorylation of pS641, pS646, pS692 and pS696 in melanoma (57), the roles of pS665 and pS681 phosphosites have not been previously characterized.

Similar to prior reports, multiple target phosphosites of MTOR showed significant upregulation in response to HRAS overexpression, including pS289 on BAG3, pS766 and pS774 on LARP1, and pS212 on AKT1S1 (1.4-fold). All three targeted proteins have been previously associated with roles in cell proliferation and anti-apoptotic activity (58, 59).

Taken together, our findings indicate that the MAPK and PI3K pathways are highly activated in RAS-NHA cells.

Other Ras Downstream Pathways—In addition to the MAPK and PI3K pathways, we identified altered phosphorylation of other pathways and proteins that are known to act downstream of RAS, such as Cdc42 effector proteins 1, 2, 3, and 4, and p21-activated kinases (PAKs), as well as several PAK target proteins. For example, multiple PAK1 target sites, including ARHGEF2 pS886 displayed upregulation (2.6-fold) (60). Furthermore, the PAK1 inhibitor Merlin (NF2) showed significant (2.8-fold) downregulation at the protein level, which is characteristic for PAK1 hyperactivation (61). We further found that several Rho guanine nucleotide exchange factors (GEFs) and Rho GTPase activating proteins (GAPs), such as ARHGEF2, ARHGEF7, ARHGEF28, and ARHGAP22, ARHGAP23, and ARHGAP24 exhibited significant upregulation of protein abundance or phosphorylation. For instance, ARHGEF2 phosphosites pS696, pS886, and pS645 demonstrated 3.2-fold and higher upregulation.

RAS related proteins RALA, RALB, and RALBP1 are important for RAS-mediated oncogenic signaling (62), and we found that 6 of the 13 identified RAL interaction partners (R-RAS2, RAP2B, RAB8B, RGL4, RALA and RALB) showed 2-fold or higher upregulation at the protein level (supplemental Fig. S5).

Therefore, in addition to MAPK and PI3K pathways, multiple other RAS effector pathways and proteins displayed changes consistent with their RAS-dependent regulation.

B) Phosphorylation Patterns Point to Feedback Mediated Phosphorylation of Upstream Regulators of RAS—In addition

to the changes in downstream effectors of RAS, we also found changes in phosphorylation of multiple proteins upstream of HRAS, pointing to feedback regulation mechanisms. For example, EGFR, FGFR4, EPHA2, and TGFBR2 receptors showed significant phosphorylation upregulation in RAS-NHA cells. EGFR phosphosites pT648, pS991, and pS1166 displayed 3.5-fold, 3.7-fold, and 1.6-fold upregulation, respectively. The pS991 and pS1166 sites are both thought to be negative regulators of EGFR (63, 64). EGFR pT648 has not been previously functionally characterized, but our results suggest that by analogy to pS991 and pS1166 this phosphosite may also be involved in feedback downregulation of EGFR. Additionally, pS251 and pS369 of ERRFI1, which is a negative regulator of EGFR (65), were also significantly upregulated, raising the possibility that phosphorylation at these sites may promote the activity of ERRFI1 as a negative regulator of EGFR.

Furthermore, we found that FGFR4 phosphorylation site pS573 was one of the most significantly upregulated (34-fold) sites in our experiment. Whether phosphorylation of pS573 on FGFR4 promotes its activation or inhibition, however, remains unclear. Interestingly, the receptor tyrosine kinases (RTKs) EPHA2 and EPHB2, which are both involved in cell adhesion and migration dependent signaling, showed distinct responses to RAS activation. Although EPHB2 didn't reveal regulation in RAS-NHA cells, EPHA2 showed significant upregulation at the protein and phosphorylation levels. The AKT-mediated EPHA2 phosphorylation on residue pS897 displayed a 4.9-fold upregulation.

C) Dual MAPK and PI3K Inhibition Yields a More Complete Reversal of the Phosphorylation Changes Driven by Oncogenic HRAS Compared with MEK Inhibition Only—We next wanted to know if the protein and phosphorylation regulation changes observed as a result of oncogenic HRAS overexpression in NHA cells could be reversed by inhibition of its downstream effects. Specifically, we sought to identify and compare the sets of regulatory changes reversible by either a MEK inhibitor alone or in combination with a PI3K inhibitor. For this purpose, we treated RAS-NHA cells with a highly selective small-molecule inhibitor of MEK1/2 (GDC-0973, Genentech Inc.) (11) and a potent class I PI3K inhibitor (GDC-0941, Genentech Inc.) (12) and measured global protein and phosphorylation changes (Fig. 5*A*).

MEK Inhibition—After MEK inhibition alone, we identified 95 and 170 phosphosites displaying at least 2-fold down or upregulation in RAS-NHA cells compared with DMSO treatment, respectively (supplemental Table S8 and supplemental Fig. S6*A*). Overall, we identified 115 (41.4%) of all significantly upregulated sites observed in the RAS-NHA *versus* control-NHA cells experiments. Although 15 (13.0%) of upregulated sites in RAS-NHA cells displayed at least 2-fold downregulation after MEK inhibition (reversible sites) (Fig. 5*B*), 25 (21.7%) were paradoxically activated upon MEK inhibition beyond that seen from HRAS overexpression (nonreversible sites) (Fig. 5*C*) (supplemental Table S9). Reversible sites that showed at least 2-fold downregulation after MEK inhibition, included MAPK1 (pY187) and MAPK3 (pY204) as well as phosphoproteins involved in RAS protein signaling transduction (FAM129B and ARHGAP29). Other reversible sites included EPS8L2 (pS459), NES (pT338), PML (pS527) and TACC1 (pS276). On the contrary, we observed nonreversible sites such as AKT1S1 (pT246), which is consistent with the compensatory activation of PI3K pathway as a result of MEK inhibition observed in other systems (66). Interestingly, NES phosphorylation sites showed opposite regulation after MEK inhibition. Although pT338 was reversible, pS905 was activated upon MEK inhibition. HMGA1 (pS44), GREM1 (pS77), and IL6ST (pS667) were also categorized as non-reversible sites. In addition to the changes in downstream proteins, we found altered phosphorylation of multiple proteins upstream of MEK pointing to feedback regulation mechanisms. For example, NGFR pS313, which already showed 16-fold upregulation in RAS-NHA cells (compared with control-NHA cells) was upregulated 20-fold more after MEK inhibition alone, suggesting that this site might be involved in compensatory activation of NGFR following MEK inhibition.

Dual MEK and PI3K Inhibition—We next investigated the efficacy of dual MEK and PI3K inhibition in reversing signaling changes mediated by oncogenic HRAS in RAS-NHA cells. By applying quantitative MS after 4 h of treatment, we found 403 phosphosites displaying at least 2-fold downregulation after dual inhibition compared with DMSO treatment. Only a minority of phosphosites (129) showed more than 2-fold upregulation after dual inhibition (supplemental Table S10 and supplemental Fig. S6*B*).

In this dual inhibition experiment, we quantified 217 (78.1%) of significantly upregulated phosphosites identified in the RAS-NHA *versus* control-NHA cells experiment. Of these, 49 (22.6%) showed significant downregulation after dual inhibition (reversible sites) (Fig. 5*D*) and 6 (2.8%) displayed significant upregulation (nonreversible sites) (Fig. 5*E*) (supplemental Table S11).

Among the reversible phosphorylation sites, MAPK1 (pT185, pY187), MAPK3 (pY90), and AKT1S1 (pT246) showed the most substantial downregulation (up to 68-fold) after dual inhibition. Furthermore, downstream targets of the MAPK signaling cascade such as pS641, pS646, pS692 and pS696 of FAM129B, ARHGAP29 pS1029, and pS405 CTTN showed significant reversed phosphorylation patterns. Multiple downstream targets of PI3K, including BAG3 and EIF4E showed significant reversed phosphorylation patterns as well. Interestingly, pS946 and pT648 of the upstream regulator EGFR were also reversed. Similar to MEK inhibition only, NES phosphorylation sites showed distinct responses to dual inhibition. Although pT338 was significantly downregulated after MEK inhibition only and dual inhibition, pS1577 was one of the few nonreversible phosphorylation sites after dual inhibition. Other nonrevers-

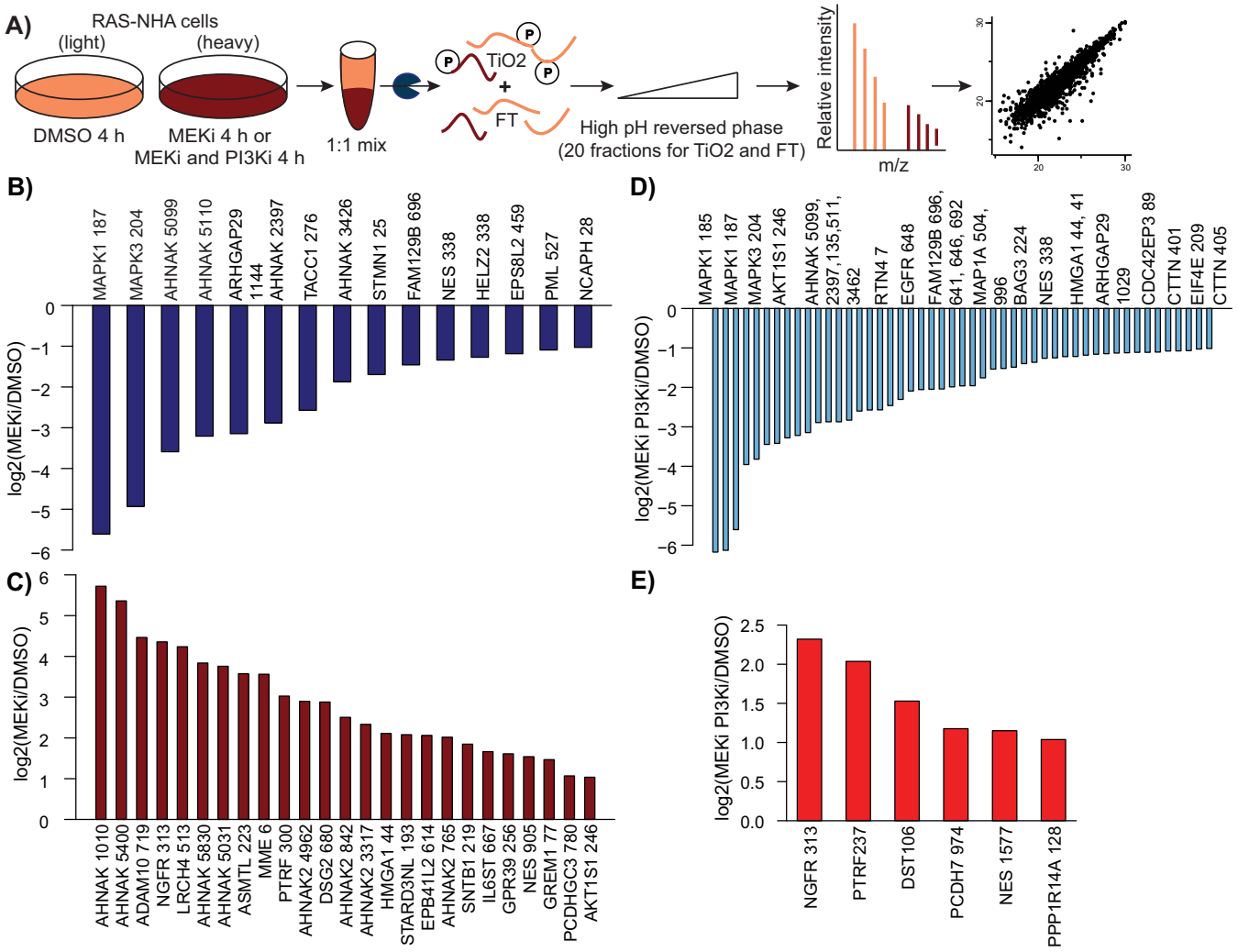

FIG. 5. **MEK and PI3K inhibition reverses phosphorylation signaling patterns driven by oncogenic HRAS overexpression in RAS-NHA cells.** *A*, Experimental overview. *B*, Down and (*C*) upregulated phosphosites after MEK inhibition that were also upregulated in RAS-NHA *versus* control-NHA cells. *D*, Down and (*E*) upregulated phosphosites after dual MEK and PI3K inhibition that were upregulated in RAS-NHA cells compared with control-NHA cells.

ible phosphosites included NGFR (pS313), PTRF (pS237), DST (pS106), PCDH7 (pS974), and PPP1R14A (pS128), suggesting that different pathways, other than PI3K and MAPK regulate these sites.

MEK Inhibition Only Versus Dual MEK and PI3K Inhibition—Comparing both experiments to each other revealed that several phosphorylation sites showed opposite or more substantial downregulation after MEK and PI3K inhibition compared with MEK inhibition alone. For example, pT246 of AKT1S1 showed 12-fold abundance-independent downregulation after dual inhibition, but 2-fold abundance-independent upregulation after MEK inhibition alone. RICTOR pS1302, which was 1.7-fold upregulated after MEK inhibition, showed no changes in phosphorylation after simultaneous inhibition. Several phosphosites of CDC42EP proteins and TGFBR2, which showed abundance-independent increased phosphorylation after MEK inhibition displayed downregulation after dual inhibition. Multiple phosphosites of IRS-1 and 2, which are known substrates of MAPK (67), showed 3.5-fold or higher downregulation after dual inhibition, but only moderate responses ($<$ 1.5-fold) after MEK inhibition. We further observed that in addition to RAS and cell cycle associated proteins, phosphosites of focal adhesions and cell motion proteins were significantly downregulated after dual inhibition compared with MEK inhibition alone (supplemental Fig. S6*C*, S6*D*, and S6*F*).

Taken together, inhibition of MEK reversed only a minority of HRAS-driven phosphorylation patterns. In comparison, simultaneous inhibition of the MAPK and PI3K signaling pathways reversed many signaling changes driven by oncogenic HRAS with the exception of six phosphorylation sites that were not reversible. Dual inhibition was clearly superior in reversing oncogenic signaling in HRAS driven glioma cells compared with MEK inhibition alone.

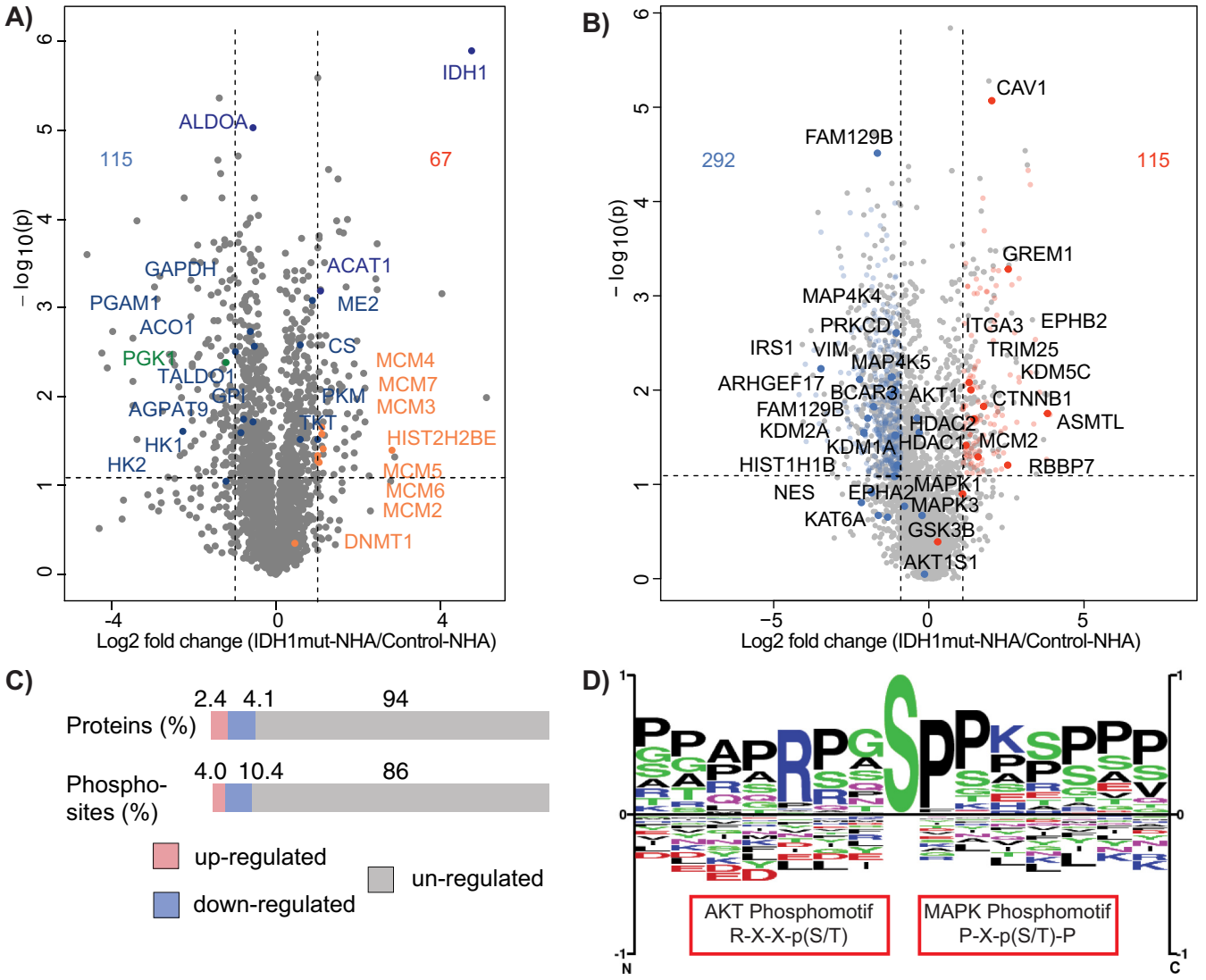

FIG. 6. **Significant dysregulation of epigenetic and metabolic proteins in IDH1mut-NHA cells.** The volcano plots illustrate the Log2 fold changes in IDH1mut-NHA compared with control-NHA cells (*x* axis) at the (*A*) protein abundance or (*B*) phosphorylation level and *p* values estimated in biological replicates (*y* axis). *C*, Proportion of regulated (at least 2-fold) proteins and phosphosites in all 3 biological replicates. *D*, Downregulated phosphosites in IDH1mut-NHA cells are enriched for MAPK and PI3K motifs compared with control cells.

III) Oncogenic Activity of Mutant IDH1 Induces Global Protein Expression Changes and Perturbs Epigenetic Regulation in IDH1mut-NHA Cells—

Global Proteome and Phosphoproteome in IDH1mut-NHA Cells—IDH1 mutation is a selective marker of secondary glioblastoma, and given its pivotal role in the inhibition of histone demethylases and reorganization of DNA methylation, we assessed whether protein abundance changes can be linked to the histone PTM signature of IDH1mut-NHA cells.

Overall, we observed more down than upregulated proteins as well as phosphorylation sites in IDH1mut-NHA cells compared with control-NHA cells. In total, 115 proteins (4.1%) and 292 phosphosites (10.4%) showed at least 2-fold downregulation compared with 67 (2.4%) proteins and 115 (4.0%) phosphosites displaying significant upregulation (Fig. 6*C* and supplemental Table S12). The observed protein abundance changes were concordant with prior transcriptomic profiling of IDH1mut-NHA cells that revealed a global downregulation of gene expression compared with wild type IDH1 (IDH1wt) NHA cells (22). Both proteomic and transcriptomic observations are consistent with the G-CIMP of IDH1 mutant gliomas, which induces global reorganization of the transcriptome (22, 68). Similar to other studies showing that mRNA expression levels are not fully reflective of protein abundances (23, 24), we found that relative protein intensities in IDH1mut-NHA cells did not correlate with relative gene expression when comparing our data with the microarray data (supplemental Fig. S7).

IDH1 Mutation Induces Epigenetic Alterations in IDH1mut-NHA Cells—Upregulated proteins in IDH1mut-NHA cells were

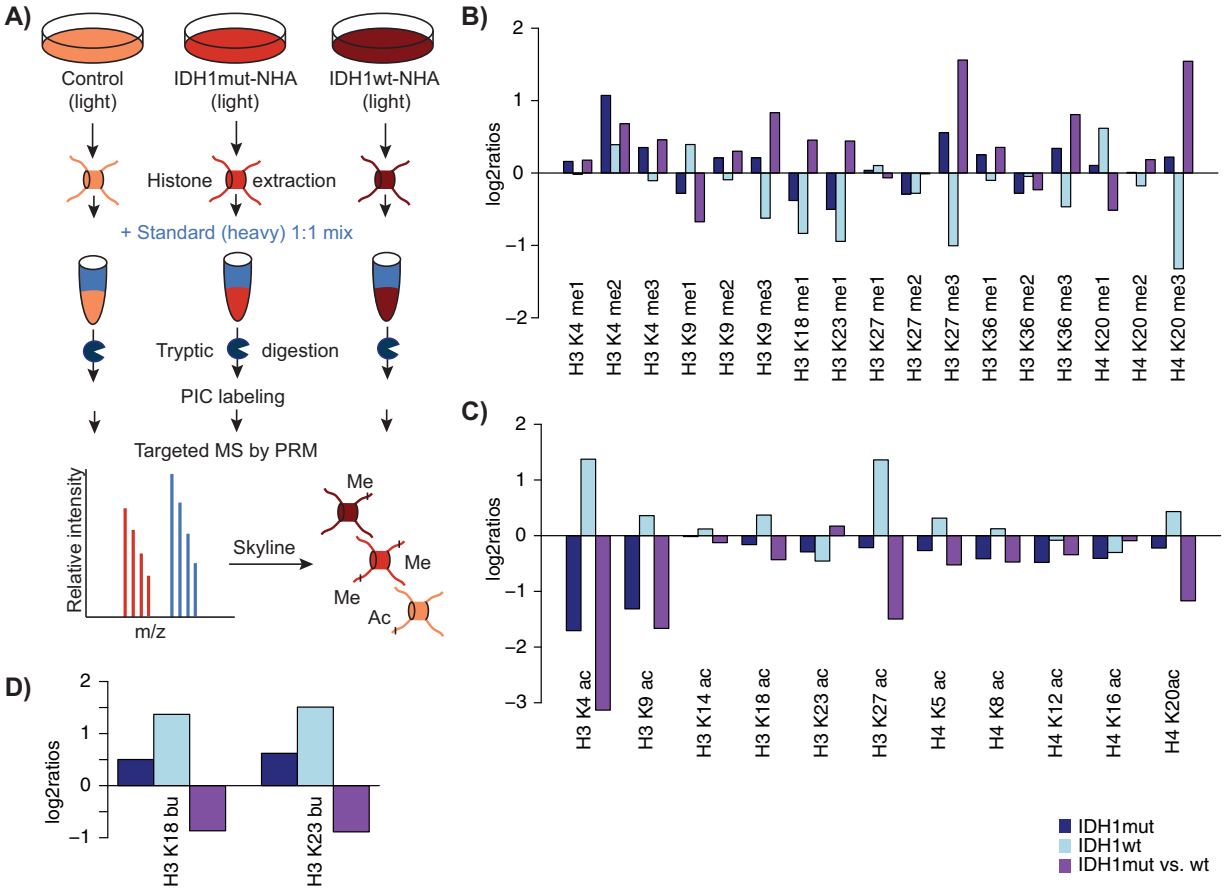

FIG. 7. **Histone PTM occupancies in IDH1mut- and IDH1wt-NHA cells.** *A*, Experimental design to assign histone PTM occupancies. The barplots illustrate histone (*B*) methylation, (*C*) acetylation, and (*D*) butyrylation changes (log2 ratios) in IDH1mut- (*dark blue*) and IDH1wt-NHA (*light blue*) compared with control-NHA cells and IDH1mut- compared with IDH1wt-NHA cells (*purple*).

enriched for chromatin-associated proteins, such as DNA replicating licensing factors MCM2–7, DNMT1, and HELLS (highlighted in orange in Fig. 6*A*). In addition, multiple chromatin-associated proteins, including α-KG-dependent KDM2A, displayed significant phosphorylation alterations (Fig. 6*B*). Interestingly, the most significantly upregulated phosphorylation site in IDH1mut-NHA cells was localized on N-acetylserotonin O-methyltransferase-like protein ASMTL (pS223) protein. Additionally, phosphosites in lysine specific demethylases KDM1A (pS166) and KDM2A (pS740) showed significant downregulation, whereas pS301 of KDM5C displayed significant upregulation.

α-KG-dependent histone demethylases are major targets of IDH1 (20, 69). Most α-KG dependent histone modifying enzymes, however, did not show significant changes in protein abundance in our dataset, suggesting that functional inhibition of α-KG dependent enzymes by mutant IDH1 does not significantly affect their protein expression level.

Histone PTM Occupancies in IDH1mut-NHA Cells Reveal a Transcriptional Silencing State—We next sought to investigate the downstream targets of α-KG dependent histone demethylases. To this end, we compared histone PTM occupancies of IDH1mut-NHA to control-NHA cells. We quantified site-specific histone PTMs by applying a hybrid chemical labeling method and MS analysis by PRM (Fig. 7*A* and supplemental Table S13).

Histone Methylation—Overall, we identified 29 different methylation marks on histone H3. Consistent with previous studies using antibody-based detection approaches (22, 70), multiple histone methylation sites showed significant increase in methylation in IDH1mut-NHA compared with control-NHA cells, including H3K9me3 (1.2-fold), H3K27me3 (1.5-fold), and H3K36me3 (1.3-fold). We further identified two other significantly upregulated tri-methylated marks on histone H3 (H3K4me3 and H4K20me3) (Fig. 7*B*). Although H3K9me3, H3K27me3, H4K20me3, and H3K36me3 are known to be associated with transcriptional silencing, H3K4me3 is linked to transcriptional activation (71). To control for possible effects of IDH1 protein overexpression, we also included IDH1wt-NHA cells in our histone PTM analysis. We found that IDH1wt-NHA cells presented opposite histone tri-methylation regulation compared with IDH1mut-NHA cells, as H3K9me3, H3K27me3, H3K36me3, and H4K20me3 displayed significant downregulation in IDH1wt-NHA cells. All three histone marks,

displayed 1.8-, 2.9-, 1.7-, and 2.9-fold increased upregulation in IDH1mut- compared with IDH1wt-NHA cells, respectively. These results are consistent with the function of wild type IDH1, which produces α-KG and subsequently activates α-KG-dependent histone demethylases. Mutant IDH1, however, inhibits α-KG-dependent histone demethylases, which results in increased histone tri-methylation.

In contrast to tri-methylated histone lysines, mono- and di-methylated lysines did not show significant regulation and appear not to be affected by mutant IDH1. Overall, the observed methylation patterns suggest a transcriptional repressive state in IDH1mut-NHA cells.

Histone Acetylation—While the majority of histone methylation marks have been linked to transcriptional repression, lysine acetylation is associated with transcriptional activation (72). We found that IDH1mut-NHA cells displayed significant downregulation of histone acetylation. In fact, all associated marks, including H3K4ac, H3K9ac, H3K23ac, H3K27ac, H4K5ac, H4K8ac, H4K12ac, H4K16ac, and H4K20ac, showed significant downregulation (Fig. 7*C*). H3K4ac and H3K9ac displayed the most significant downregulation (8.6-fold and 3.1-fold compared with IDH1wt-NHA cells, respectively). Both of these marks, if acetylated, are known to induce transcriptional activation (73, 74). Finally, H3K14ac and H3K18ac showed a trend for downregulation in IDH1mut-NHA cells. These results indicate that mutant IDH1 induces a global transcriptional state through reduced acetylation.

Histone Butyrylation—Among all identified histone PTMs, butyrylation was one of the most upregulated marks. We identified three histone butyrylation sites on histone H3 (H3K14, H3K18, and H3K23). The H3K18 and H3K23 butyrylation marks displayed 1.4-fold and 1.5-fold upregulation in IDH1mut-NHA cells compared with control cells, respectively (Fig. 7*D*). Histone butyrylation, however, was even more significantly upregulated in IDH1wt-NHA cells. In fact, histone butyrylation was 1.9-fold downregulated in IDH1mut- compared with IDH1wt-NHA cells. These observations suggest a regulatory link between IDH1 mutation and histone butyrylation.

In summary, our histone PTM analysis revealed a significant upregulation of histone lysine trimethylation and downregulation of histone acetylation and butyrylation in IDH1mut-NHA cells compared with IDH1wt-NHA cells, pointing to a global transcriptional repressive state mediated by mutant IDH1, consistent with the observed downregulated proteome in IDH1mut-NHA cells.

Mutant IDH1 Induces Metabolic Changes in IDH1mut-NHA Cells—In addition to epigenetic changes, we found that metabolic proteins (highlighted in blue in Fig. 6*A* and supplemental Fig. S8) regulating glycolysis, lipolysis, as well as oxidoreductase activity were significantly dysregulated in IDH1mut-NHA cells compared with control-NHA cells. Although metabolic proteins AGPAT9, ACO1, GAPDH, PGAM1, TALDO1, ALDOA, HK1, HK2, and GPI displayed downregulation, ACAT1, ME2, CS, TKT, and PKM were significantly upregulated. Changes in glucose flux in IDH1mut-NHA cells were reflected by the downregulation of the AKT pathway (Fig. 6*D*) and other enzymes stimulating the glycolytic flux, such as hexokinases. These findings have also been observed in a label free analysis, comparing the proteomes of IDH1mut-NHA to control-NHA cells in a single-run mass spectrometry workflow (supplemental Fig. S8). These observations are concordant with the pivotal role of IDH1 within the TCA cycle (75).

IV) HRAS-overexpressing or IDH1-mutated Astrocytomas Are Driven by Different Oncogenic Pathways—We showed that both RAS-NHA and IDH1mut-NHA cells express dysregulated altered oncogenic pathways. Using PCA, both cell lines can be clearly differentiated from each other based on their proteomic and phosphoproteomic profiles (supplemental Fig. S9). The driving role of the MAPK and PI3K pathways in RAS-NHA cells was not reflected in IDH1mut-NHA cells. The surrounding sequences of downregulated phosphosites in IDH1mut-NHA cells significantly matched with canonical MAPK substrate recognition motifs (Fig. 6*D*). Concordantly, downstream targets of the MAPK signaling cascade such as pS641, pS646, pS692 and pS696 of FAM129B (57), which displayed significant upregulation in RAS-NHA cells, showed significant downregulation in IDH1mut-NHA cells. In addition, PI3K targets, such as AKT1S1 pT246 did not reveal any regulation in IDH1mut-NHA cells (Fig. 6*B*).

Other signaling pathways that showed different regulation in IDH1mut- compared with RAS-NHA cells include the Wnt pathway. IDH1mut-NHA cells displayed significant upregulation of β-catenin phosphosites and no upregulation of the AKT-mediated inactivating GSK3β pS9 phosphorylation site, indicating an inactive or less active Wnt signaling pathway compared with RAS-NHA cells (supplemental Fig. S10). This finding is consistent with a recent report highlighting that IDH1 Arg132 mutation reduces cell proliferation by downregulating Wnt/β-Catenin signaling in glioblastoma (76). Although the role of the Wnt pathway in human glioma remains unclear, the Wnt pathway has oncogenic (77, 78) and antioncogenic (79–81) activities in several cancer types.

Interestingly, one of the most downregulated (7-fold) proteins in IDH1mut-NHA cells was NES, which showed opposite regulation in RAS-NHA cells with a 10-fold upregulation at the protein level. We further showed by label free MS analysis and Western blot that NES was exclusively downregulated in IDH1mut-NHA cells when compared with IDH1wt-NHA, RAS-NHA, or control cells (supplemental Table S14 and supplemental Fig. S11). NES has been previously reported to be overexpressed in GBM (27), to correlate with the malignancy of glioblastoma (82), and its inhibition significantly reduced tumor growth (83).

At the cell membrane level, EPHA2 and EPHB2 showed distinct responses to RAS activation or IDH1 mutation in our experiments. Although EPHA2 showed significant upregulation in RAS-NHA cells, no significant changes were observed

in IDH1mut-NHA cells. EPHB2, however, revealed significant upregulation at the protein and phosphosite level exclusively in IDH1mut-NHA cells.

To assess the involvement of identified proteins in cancer we compared our phosphoproteomic and proteomic data to a catalogue of 150 tumor suppressor genes and 350 oncogenes listed in the cancer gene census (84). Overall, we quantitated the relative abundance of 33 tumor suppressor proteins (TSPs) and 102 oncoproteins in our proteomic or phosphoproteomic experiments. Among the TSPs, Neurofibromin (NF1) and NF2 showed the most significant downregulation of both abundance and phosphorylation in RAS-NHA cells but did not show any significant regulation in IDH1mut-NHA cells. At the abundance level, NF1 (identified in one of the three biological replicates) and NF2 displayed 9-fold and 2.8-fold downregulation, respectively. NF1 and NF2 have been shown to inhibit the activity of HRAS but not vice-versa (85–88). Loss of NF1 subsequently results in the activation of multiple pathways involved in gliomagenesis, including the MAPK and PI3K pathways (89). The regulatory role of NF2, however, remains poorly understood (90). Downregulated phosphorylation sites included pS864, pS2523 (2.6-fold), pS2543 (4.6-fold) on NF1 and pS13 (2.8-fold) on NF2 proteins. The downregulated phosphosites of NF1 have been previously reported, but their function is unknown. In particular, all three phosphorylation residues we uncovered on NF2 including pS10, pS12, and pS13 have not been characterized, pointing to previously unknown regulatory mechanisms.

Conclusion and Outlook—In the present study we used SILAC-based MS to characterize global phosphorylation and protein abundance changes in immortalized NHA cells expressing oncogenic HRAS or mutant IDH1. Although these two models are not fully reflective of primary and secondary GBM, they showed very distinct proteomic profiles consistent with fundamentally different biological programs driving tumorigenesis in primary and secondary GBM (Fig. 8).

In RAS-NHA cells, we found activation of MAPK and PI3K pathways. In addition to known changes in MAPK and PI3K pathways, we identified significant changes in previously uncharacterized phosphosites within these pathways implicating them as likely sites of regulation downstream of oncogenic HRAS signaling. These include EIF4E, FAM129A, FAM129B, PAK, and NF2.

MEK inhibition resulted in partial reversibility of the changes driven by oncogenic HRAS, whereas dual MAPK and PI3K inhibition yielded a more complete reversal. Some compensatory changes because of MEK inhibition as a single agent, including PI3K activation and upstream regulators TGFBR2 and EGFR were blocked by the dual inhibition. However, even dual MEK and PI3K inhibition did not reverse all signaling changes mediated by oncogenic HRAS. NES (pS1577), NGFR (pS313), PTRF (pS237), DST (pS106), PCDH7 (pS974), and PPP1R14A (pS128) were some of the few non-reversible phosphorylation sites after dual inhibition, suggesting that previously unknown feedback mechanisms regulate these sites. Although dual inhibition of MEK and PI3K is clearly superior to single MEK inhibition and is currently in phase I clinical trials, based on these findings and multiple other studies, clinical efficacy remains to be determined (91).

In addition to the activation of MAPK and PI3K pathways in RAS-NHA cells, we identified changes in several other pathways. We observed a potential driving role for PAKs in glioma development, consistent with previous studies (92–94). We further found several interaction partners of the RAL proteins, which are commonly over-expressed in multiple cancer types, including glioblastoma, to be highly upregulated in RAS-NHA cells (62) (95, 96). In addition to regulation of the main signaling cascades downstream of RAS, we observed substantial phosphorylation and protein expression changes in other pathways such as the Wnt pathway, presumably triggered by interplay between the cascades. We also found regulated phosphorylation sites of multiple proteins upstream of RAS, pointing to feedback mechanisms. For instance, the FGF signaling pathway, in particular FGFR4, which showed massive upregulation at the phosphorylation level has been reported to stimulate the growth of GBM (97). We also identified activating phosphorylation sites on EPHA2, which have been associated with glioblastoma invasion, consistent with the malignant phenotype of RAS-NHA cells (98). EPHA2 and other Ephrin family receptors are particularly attractive for targeted therapy, because they are expressed at very low abundance or not expressed in healthy tissues but show high expression in most cancerous tissues (99).

Unlike the changes in RAS-NHA cells characterized by dysregulation of major signaling pathways, IDH1mut-NHA cells displayed a global downregulation of protein expression, detected at the level of both protein abundance and phosphorylation. The overall downregulation of protein expression is consistent with evidence of genome-scale transcriptional silencing identified previously (22). Protein expression changes were accompanied by changes in histone PTMs, pointing to transcriptional repression, which in turn results from mutant IDH1-mediated inhibition of histone demethylases. Our histone PTM analysis revealed a significant upregulation of tri-methylated histone lysines, which are known to be demethylated exclusively by α-KG-dependent histone demethylases. Therefore, our data suggest that α-KG dependent histone demethylases are inhibited in IDH1mut-NHA cells. This observation is consistent with previous reports that demonstrated the overproduction of 2-HG, acting as a competitive inhibitor of α-KG-dependent enzymes in IDH1mut-NHA cells (18). Increase in methylation was accompanied by a decrease in acetylation at essentially all measured sites providing further support for a state of global transcriptional repression mediated by mutant IDH1. We speculate that histone deacetylase (HDAC) inhibitors, including those currently in clinical trials for the treatment of GBM (100), may reverse the downregulation of the histone acetylome in IDH1mut-NHA

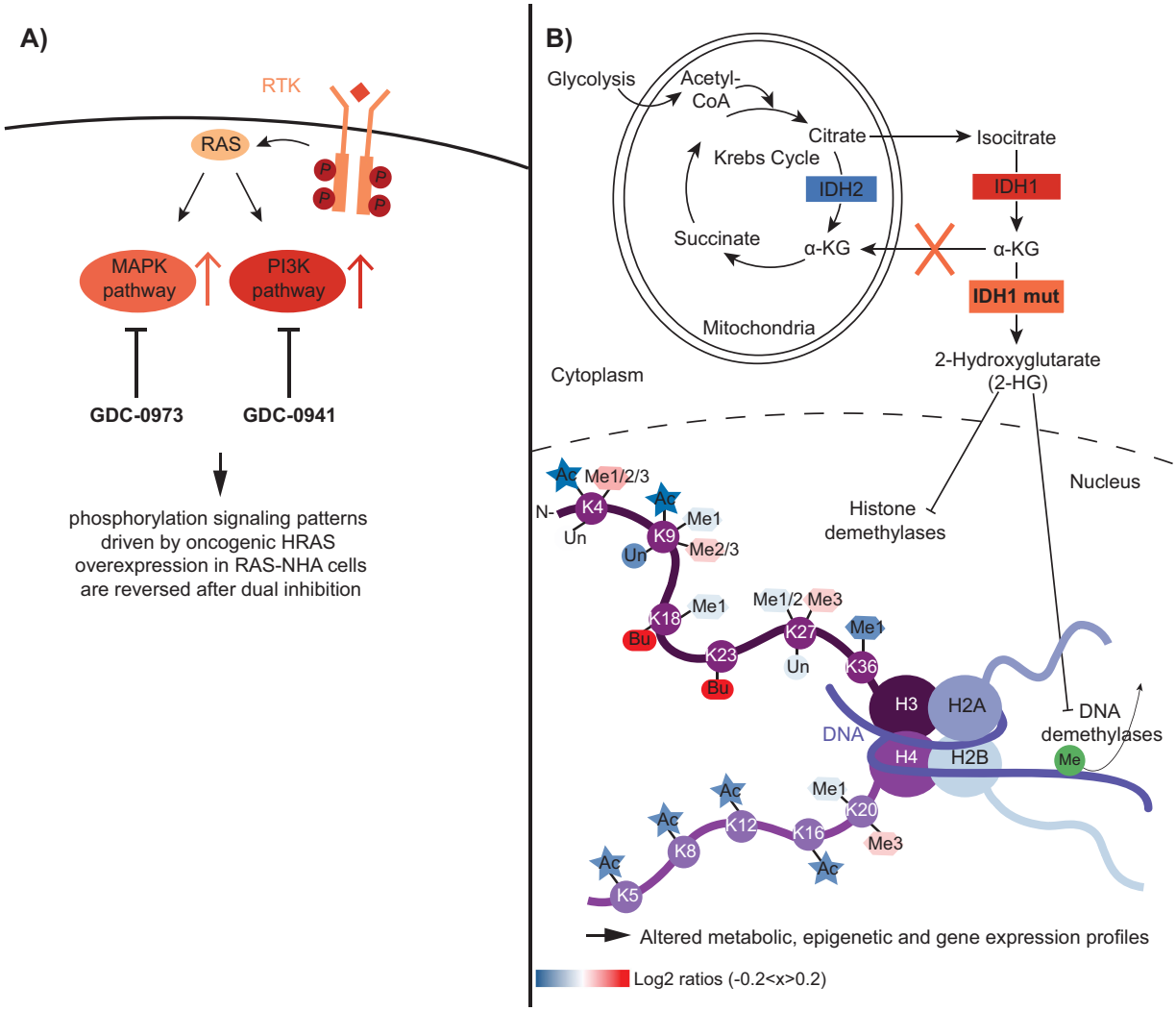

FIG. 8. **Schematic summary of the role of HRAS and IDH1 mutation in astrocytoma cell lines.** *A*, MAPK and PI3K pathways play a pivotal role in RAS-NHA cells *B*, IDH1 mutation induces epigenetic alterations. Although histone tri-methylation marks and butyrylation display significant upregulation, histone acetylation marks present significant downregulation in IDH1mut-NHA cells.

cells. We also detected upregulation of histone butyrylation in IDH1mut- and IDH1wt-NHA cells. However, when compared with IDH1wt-, IDH1mut-NHA cells displayed downregulated histone butyrylation changes. The function of this recently discovered histone PTM (101) remains largely unknown. A study showed that butyrate and free CoA inhibit the activity of HDACs but conjugated butyryl-CoA stimulated the activity of HDACs (102). These findings suggest that IDH1mut-NHA cells present decreased butyryl-CoA concentrations compared with IDH1wt-NHA cells. It remains unknown, however, if besides p300/CBP (101) other histone acetyl transferases can use in addition to acetyl-CoA, other short-chain CoAs, such as butytyl-CoA to carry out lysine butyrylation or whether HDACs can debutyrylate lysines. Our results suggest that histone butyrylation is regulated by different enzymes or mechanisms than histone acetylation. Targeted PRM-based MS is particularly suitable for the decryption of histone PTM occupancies compared with antibody-based methods, which are commonly hindered by low specificity - in particular toward di- and tri-methylated lysines - and epitope occlusion problems, preventing the detection of combinatorial marks. To investigate histone PTM occupancies in more detail, alternative quantification approaches, including electron transfer MS methodology could be applied. These methods investigate entire histones or large peptides directly by electron transfer dissociation MS (103, 104). Although these analytical strategies lack precise quantification and sensitivity, they would provide complimentary information and be suitable for follow up studies.

In summary, we provide integrated comparison of the proteomic changes in HRAS and IDH1mut driven malignant astrocytoma cells, which points to drastically different gliomagenesis mechanisms in primary and secondary GBM. Our analysis includes, to the best of our knowledge, the first

targeted MS-based demonstration of multiple histone PTM changes driven by mutant IDH1 in a cellular model of secondary glioblastoma. Based on these biological observations, we predict very different therapeutic interventions to be useful in primary *versus* secondary GBM. We provide a valuable resource of proteins altered in glioma, including potential biomarkers or therapeutic targets.

Acknowledgments—We thank R. O. Pieper and J. Mukherjee for helpful discussions and providing immortalized human astrocytes, T. Maile for help with the analysis of histone PTMs and R. Levin for helpful input.

* This work was supported by National Institutes of Health/National Institute of General Medical Sciences (NIH/NIGMS) grant 8P41GM103481 and the Adelson Medical Research Foundation. The Howard Hughes Medical Institute (HHMI) contributed to the purchase of the LTQ-Orbitrap Velos. The content is solely the responsibility of the authors and does not necessarily represent the official views of the National Institutes of Health.

[S] This article contains supplemental material.

‖ Current address: Dept. of Proteomics and Signal Transduction, Max Planck Institute of Biochemistry, Martinsried, Germany.

¶ To whom correspondence should be addressed: Pharmaceutical Chemistry Institution, University of California, San Francisco, 600 16th Street Genentech Hall N472, Box 2240, San Francisco, CA 94158-2517. Tel.: 415-476 5641; Fax: 415-502 1655; E-mail: alb@cgl.ucsf.edu.

REFERENCES

1. Ferlay, J., Soerjomataram, I., Dikshit, R., Eser, S., Mathers, C., Rebelo, M., Parkin, D. M., Forman, D., and Bray, F. (2015) Cancer incidence and mortality worldwide: Sources, methods and major patterns in GLOBOCAN 2012: Globocan 2012. *Int. J. Cancer* **136,** E359-E386
2. Furnari, F. B., Fenton, T., Bachoo, R. M., Mukasa, A., Stommel, J. M., Stegh, A., Hahn, W. C., Ligon, K. L., Louis, D. N., Brennan, C., Chin, L., DePinho, R. A., and Cavenee, W. K. (2007) Malignant astrocytic glioma: genetics, biology, and paths to treatment. *Genes Dev.* **21,** 2683–2710
3. Louis, D. N., Ohgaki, H., Wiestler, O. D., Cavenee, W. K., Burger, P. C., Jouvet, A., Scheithauer, B. W., and Kleihues, P. (2007) The 2007 WHO classification of tumours of the central nervous system. *Acta Neuropathol.* **114**, 97–109
4. Ostrom, Q. T., Gittleman, H., Liao, P., Rouse, C., Chen, Y., Dowling, J., Wolinsky, Y., Kruchko, C., and Barnholtz-Sloan, J. (2014) CBTRUS statistical report: Primary brain and central nervous system tumors diagnosed in the United States in 2007–2011. *Neuro-Oncol.* **16**, iv1–iv63
5. Ohgaki, H., and Kleihues, P. (2013) The Definition of Primary and Secondary Glioblastoma. *Clin. Cancer Res.* **19,** 764–772
6. Brennan, C. W., Verhaak, R. G. W., McKenna, A., Campos, B., Noushmehr, H., Salama, S. R., Zheng, S., Chakravarty, D., Sanborn, J. Z., Berman, S. H., Beroukhim, R., Bernard, B., Wu, C.-J., Genovese, G., Shmulevich, I., Barnholtz-Sloan, J., Zou, L., Vegesna, R., Shukla, S. A., Ciriello, G., Yung, W., Zhang, W., Sougnez, C., Mikkelsen, T., Aldape, K., Bigner, D. D., Van Meir, E. G., Prados, M., Sloan, A., Black, K. L., Eschbacher, J., Finocchiaro, G., Friedman, W., Andrews, D. W., Guha, A., Iacocca, M., O'Neill, B. P., Foltz, G., Myers, J., Weisenberger, D. J., Penny, R., Kucherlapati, R., Perou, C. M., Hayes, D. N., Gibbs, R., Marra, M., Mills, G. B., Lander, E., Spellman, P., Wilson, R., Sander, C., Weinstein, J., Meyerson, M., Gabriel, S., Laird, P. W., Haussler, D., Getz, G., and Chin, L. (2013) The somatic genomic landscape of glioblastoma. *Cell* **155,** 462–477
7. Sonoda, Y., Ozawa, T., Hirose, Y., Aldape, K. D., McMahon, M., Berger, M. S., and Pieper, R. O. (2001) Formation of intracranial tumors by genetically modified human astrocytes defines four pathways critical in the development of human anaplastic astrocytoma. *Cancer Res.* **61,** 4956–4960
8. Feldkamp, M. M., Lala, P., Lau, N., Roncari, L., and Guha, A. (1999) Expression of activated epidermal growth factor receptors, Ras-guanosine triphosphate, and mitogen-activated protein kinase in human glioblastoma multiforme specimens. *Neurosurgery* **45,** 1442–1453
9. Prabhu, A., Sarcar, B., Miller, C. R., Kim, S.-H., Nakano, I., Forsyth, P., and Chinnaiyan, P. (2015) Ras-mediated modulation of pyruvate dehydrogenase activity regulates mitochondrial reserve capacity and contributes to glioblastoma tumorigenesis. *Neuro-Oncol.* **17,** 1220–1230
10. Guha, A., Feldkamp, M. M., Lau, N., Boss, G., and Pawson, A. (1997) Proliferation of human malignant astrocytomas is dependent on Ras activation. *Oncogene* **15,** 2755–2765
11. Rice, K. D., Aay, N., Anand, N. K., Blazey, C. M., Bowles, O. J., Bussenius, J., Costanzo, S., Curtis, J. K., Defina, S. C., Dubenko, L., Engst, S., Joshi, A. A., Kennedy, A. R., Kim, A. I., Koltun, E. S., Lougheed, J. C., Manalo, J.-C. L., Martini, J.-F., Nuss, J. M., Peto, C. J., Tsang, T. H., Yu, P., and Johnston, S. (2012) Novel Carboxamide-Based Allosteric MEK Inhibitors: Discovery and Optimization Efforts toward XL518 (GDC-0973). *ACS Med. Chem. Lett.* **3,** 416–421
12. Folkes, A. J., Ahmadi, K., Alderton, W. K., Alix, S., Baker, S. J., Box, G., Chuckowree, I. S., Clarke, P. A., Depledge, P., Eccles, S. A., Friedman, L. S., Hayes, A., Hancox, T. C., Kugendradas, A., Lensun, L., Moore, P., Olivero, A. G., Pang, J., Patel, S., Pergl-Wilson, G. H., Raynaud, F. I., Robson, A., Saghir, N., Salphati, L., Sohal, S., Ultsch, M. H., Valenti, M., Wallweber, H. J. A., Wan, N. C., Wiesmann, C., Workman, P., Zhyvoloup, A., Zvelebil, M. J., and Shuttleworth, S. J. (2008) The identification of 2-(1H-indazol-4-yl)-6-(4-methanesulfonyl-piperazin-1-ylmethyl)-4-morpholin-4-yl-thieno[3,2-d]pyrimidine (GDC-0941) as a potent, selective, orally bioavailable inhibitor of class I PI3 kinase for the treatment of cancer. *J. Med. Chem.* **51,** 5522–5532
13. Wu, S., Wang, S., Zheng, S., Verhaak, R., Koul, D., and Yung, W. K. A. (2016) MSK1-Mediated β-catenin phosphorylation confers resistance to PI3K/mTOR inhibitors in glioblastoma. *Mol. Cancer Ther.* **15,** 1656–1668
14. El Meskini, R., Iacovelli, A. J., Kulaga, A., Gumprecht, M., Martin, P. L., Baran, M., Householder, D. B., Van Dyke, T., and Weaver Ohler, Z. (2015) A preclinical orthotopic model for glioblastoma recapitulates key features of human tumors and demonstrates sensitivity to a combination of MEK and PI3K pathway inhibitors. *Dis. Model. Mech.* **8,** 45–56
15. Parsons, D. W., Jones, S., Zhang, X., Lin, J. C.-H., Leary, R. J., Angenendt, P., Mankoo, P., Carter, H., Siu, I.-M., Gallia, G. L., Olivi, A., McLendon, R., Rasheed, B. A., Keir, S., Nikolskaya, T., Nikolsky, Y., Busam, D. A., Tekleab, H., Diaz, L. A., Hartigan, J., Smith, D. R., Strausberg, R. L., Marie, S. K. N., Shinjo, S. M. O., Yan, H., Riggins, G. J., Bigner, D. D., Karchin, R., Papadopoulos, N., Parmigiani, G., Vogelstein, B., Velculescu, V. E., and Kinzler, K. W. (2008) An integrated genomic analysis of human glioblastoma multiforme. *Science* **321,** 1807
16. Cohen, A., Holmen, S., and Colman, H. (2013) IDH1 and IDH2 mutations in gliomas. *Curr. Neurol. Neurosci. Rep.* **13,** 345
17. Yan, H., Parsons, D. W., Jin, G., McLendon, R., Rasheed, B. A., Yuan, W., Kos, I., Batinic-Haberle, I., Jones, S., Riggins, G. J., Friedman, H., Friedman, A., Reardon, D., Herndon, J., Kinzler, K. W., Velculescu, V. E., Vogelstein, B., and Bigner, D. D. (2009) IDH1 and IDH2 mutations in gliomas. *N. Engl. J. Med.* **360,** 765–773
18. Dang, L., White, D. W., Gross, S., Bennett, B. D., Bittinger, M. A., Driggers, E. M., Fantin, V. R., Jang, H. G., Jin, S., Keenan, M. C., Marks, K. M., Prins, R. M., Ward, P. S., Yen, K. E., Liau, L. M., Rabinowitz, J. D., Cantley, L. C., Thompson, C. B., Vander Heiden, M. G., and Su, S. M. (2010) Cancer-associated IDH1 mutations produce 2-hydroxyglutarate. *Nature* **465,** 966
19. Xu, W., Yang, H., Liu, Y., Yang, Y., Wang, P., Kim, S.-H., Ito, S., Yang, C., Wang, P., Xiao, M.-T., Liu, L., Jiang, W., Liu, J., Zhang, J., Wang, B., Frye, S., Zhang, Y., Xu, Y., Lei, Q., Guan, K.-L., Zhao, S., and Xiong, Y. (2011) Oncometabolite 2-hydroxyglutarate is a competitive inhibitor of α-ketoglutarate-dependent dioxygenases. *Cancer Cell* **19,** 17–30
20. Chowdhury, R., Yeoh, K. K., Tian, Y.-M., Hillringhaus, L., Bagg, E. A., Rose, N. R., Leung, I. K. H., Li, X. S., Woon, E. C. Y., Yang, M., McDonough, M. A., King, O. N., Clifton, I. J., Klose, R. J., Claridge, T. D. W., Ratcliffe, P. J., Schofield, C. J., and Kawamura, A. (2011) The oncometabolite 2-hydroxyglutarate inhibits histone lysine demethylases. *EMBO Rep.* **12,** 463–469
21. Rose, N. R., McDonough, M. A., King, O. N. F., Kawamura, A., and Schofield, C. J. (2011) Inhibition of 2-oxoglutarate dependent oxygenases. *Chem. Soc. Rev.* **40,** 4364–4397

22. Turcan, S., Rohle, D., Goenka, A., Walsh, L. A., Fang, F., Yilmaz, E., Campos, C., Fabius, A. W. M., Lu, C., Ward, P. S., Thompson, C. B., Kaufman, A., Guryanova, O., Levine, R., Heguy, A., Viale, A., Morris, L. G. T., Huse, J. T., Mellinghoff, I. K., and Chan, T. A. (2012) IDH1 mutation is sufficient to establish the glioma hypermethylator phenotype. *Nature* **483,** 479–483
23. Nagaraj, N., Wisniewski, J. R., Geiger, T., Cox, J., Kircher, M., Kelso, J., Pääbo, S., and Mann, M. (2011) Deep proteome and transcriptome mapping of a human cancer cell line. *Mol. Syst. Biol.* **7,** 548
24. Maier, T., Güell, M., and Serrano, L. (2009) Correlation of mRNA and protein in complex biological samples. *FEBS Lett.* **583,** 3966–3973
25. Johnson, H., and White, F. M. (2014) Quantitative analysis of signaling networks across differentially embedded tumors highlights interpatient heterogeneity in human glioblastoma. *J. Proteome Res.* **13,** 4581–4593
26. Nilsson, C. L., Dillon, R., Devakumar, A., Shi, S. D.-H., Greig, M., Rogers, J. C., Krastins, B., Rosenblatt, M., Kilmer, G., Major, M., Kaboord, B. J., Sarracino, D., Rezai, T., Prakash, A., Lopez, M., Ji, Y., Priebe, W., Lang, F. F., Colman, H., and Conrad, C. A. (2010) Quantitative phosphoproteomic analysis of the STAT3/IL-6/HIF1α signaling network: an initial study in GSC11 glioblastoma stem cells. *J. Proteome Res.* **9,** 430–443
27. Heroux, M. S., Chesnik, M. A., Halligan, B. D., Al-Gizawiy, M., Connelly, J. M., Mueller, W. M., Rand, S. D., Cochran, E. J., LaViolette, P. S., Malkin, M. G., Schmainda, K. M., and Mirza, S. P. (2014) Comprehensive characterization of glioblastoma tumor tissues for biomarker identification using mass spectrometry-based label-free quantitative proteomics. *Physiol. Genomics* **46,** 467–481
28. Olsen, J. V., Blagoev, B., Gnad, F., Macek, B., Kumar, C., Mortensen, P., and Mann, M. (2006) Global, in vivo, and site-specific phosphorylation dynamics in signaling networks. *Cell* **127,** 635–648
29. Ohba, S., Mukherjee, J., See, W. L., and Pieper, R. O. (2014) Mutant IDH1-driven cellular transformation increases RAD51-mediated homologous recombination and temozolomide resistance. *Cancer Res.* **74,** 4836–4844
30. Sonoda, Y., Ozawa, T., Aldape, K. D., Deen, D. F., Berger, M. S., and Pieper, R. O. (2001) Akt pathway activation converts anaplastic astrocytoma to glioblastoma multiforme in a human astrocyte model of glioma. *Cancer Res.* **61,** 6674–6678
31. Hoeflich, K. P., Merchant, M., Orr, C., Chan, J., Otter, D. D., Berry, L., Kasman, I., Koeppen, H., Rice, K., Yang, N.-Y., Engst, S., Johnston, S., Friedman, L. S., and Belvin, M. (2012) Intermittent administration of MEK inhibitor GDC-0973 plus PI3K inhibitor GDC-0941 triggers robust apoptosis and tumor growth inhibition. *Cancer Res.* **72,** 210–219
32. Sos, M. L., Levin, R. S., Gordan, J. D., Oses-Prieto, J. A., Webber, J. T., Salt, M., Hann, B., Burlingame, A. L., McCormick, F., Bandyopadhyay, S., and Shokat, K. M. (2014) Oncogene mimicry as a mechanism of primary resistance to BRAF inhibitors. *Cell Rep.* **8,** 1037–1048
33. Huang, D. W., Sherman, B. T., and Lempicki, R. A. (2008) Systematic and integrative analysis of large gene lists using DAVID bioinformatics resources. *Nat. Protoc.* **4,** 44–57
34. Subramanian, A., Tamayo, P., Mootha, V. K., Mukherjee, S., Ebert, B. L., Gillette, M. A., Paulovich, A., Pomeroy, S. L., Golub, T. R., Lander, E. S., and Mesirov, J. P. (2005) Gene set enrichment analysis: A knowledge-based approach for interpreting genome-wide expression profiles. *Proc. Natl. Acad. Sci. U.S.A.* **102,** 15545–15550
35. Deeb, S. J., Tyanova, S., Hummel, M., Schmidt-Supprian, M., Cox, J., and Mann, M. (2015) Machine learning-based classification of diffuse large B-cell lymphoma patients by their protein expression profiles. *Mol. Cell. Proteomics MCP* **14,** 2947–2960
36. Maile, T. M., Izrael-Tomasevic, A., Cheung, T., Guler, G. D., Tindell, C., Masselot, A., Liang, J., Zhao, F., Trojer, P., Classon, M., and Arnott, D. (2015) Mass spectrometric quantification of histone post-translational modifications by a hybrid chemical labeling method. *Mol. Cell. Proteomics* **14,** 1148–1158
37. Vinogradova, M., Gehling, V. S., Gustafson, A., Arora, S., Tindell, C. A., Wilson, C., Williamson, K. E., Guler, G. D., Gangurde, P., Manieri, W., Busby, J., Flynn, E. M., Lan, F., Kim, H., Odate, S., Cochran, A. G., Liu, Y., Wongchenko, M., Yang, Y., Cheung, T. K., Maile, T. M., Lau, T., Costa, M., Hegde, G. V., Jackson, E., Pitti, R., Arnott, D., Bailey, C., Bellon, S., Cummings, R. T., Albrecht, B. K., Harmange, J.-C., Kiefer, J. R., Trojer, P., and Classon, M. (2016) An inhibitor of KDM5 demethylases reduces survival of drug-tolerant cancer cells. *Nat. Chem. Biol.* **12,** 531–538
38. MacLean, B., Tomazela, D. M., Shulman, N., Chambers, M., Finney, G. L., Frewen, B., Kern, R., Tabb, D. L., Liebler, D. C., and MacCoss, M. J. (2010) Skyline: an open source document editor for creating and analyzing targeted proteomics experiments. *Bioinformatics* **26,** 966–968
39. Ong, S.-E., Blagoev, B., Kratchmarova, I., Kristensen, D. B., Steen, H., Pandey, A., and Mann, M. (2002) Stable isotope labeling by amino acids in cell culture, SILAC, as a simple and accurate approach to expression proteomics. *Mol. Cell. Proteomics* **1,** 376–386
40. Wang, W., Chen, J. X., Liao, R., Deng, Q., Zhou, J. J., Huang, S., and Sun, P. (2002) Sequential activation of the MEK-extracellular signal-regulated kinase and MKK3/6-p38 mitogen-activated protein kinase pathways mediates oncogenic ras-induced premature senescence. *Mol. Cell. Biol.* **22,** 3389–3403
41. Payne, D. M., Rossomando, A. J., Martino, P., Erickson, A. K., Her, J. H., Shabanowitz, J., Hunt, D. F., Weber, M. J., and Sturgill, T. W. (1991) Identification of the regulatory phosphorylation sites in pp42/mitogen-activated protein kinase (MAP kinase). *EMBO J.* **10,** 885–892
42. Butch, E. R., and Guan, K.-L. (1996) Characterization of ERK1 Activation site mutants and the effect on recognition by MEK1 and MEK2. *J. Biol. Chem.* **271,** 4230–4235
43. Kim, H. J., and Bar-Sagi, D. (2004) Modulation of signalling by Sprouty: a developing story. *Nat. Rev. Mol. Cell Biol.* **5,** 441–450
44. Ozaki, K., Kadomoto, R., Asato, K., Tanimura, S., Itoh, N., and Kohno, M. (2001) ERK pathway positively regulates the expression of sprouty genes. *Biochem. Biophys. Res. Commun.* **285,** 1084–1088
45. Olsen, J. V., Vermeulen, M., Santamaria, A., Kumar, C., Miller, M. L., Jensen, L. J., Gnad, F., Cox, J., Jensen, T. S., Nigg, E. A., Brunak, S., and Mann, M. (2010) Quantitative phosphoproteomics reveals widespread full phosphorylation site occupancy during mitosis. *Sci. Signal.* 3, ra3
46. Wang, L., Harris, T. E., and Lawrence, J. C. (2008) Regulation of Proline-rich Akt Substrate of 40 kDa (PRAS40) Function by mammalian target of rapamycin complex 1 (mTORC1)-mediated phosphorylation. *J. Biol. Chem.* **283,** 15619–15627
47. Foster, K. G., Acosta-Jaquez, H. A., Romeo, Y., Ekim, B., Soliman, G. A., Carriere, A., Roux, P. P., Ballif, B. A., and Fingar, D. C. (2010) Regulation of mTOR complex 1 (mTORC1) by raptor Ser863 and multisite phosphorylation. *J. Biol. Chem.* **285,** 80–94
48. Shahbazian, D., Parsyan, A., Petroulakis, E., Topisirovic, I., Martineau, Y., Gibbs, B. F., Svitkin, Y., and Sonenberg, N. (2010) Control of cell survival and proliferation by mammalian eukaryotic initiation factor 4B. *Mol. Cell. Biol.* **30,** 1478–1485
49. Raught, B., and Gingras, A.-C. (1999) eIF4E activity is regulated at multiple levels. *Int. J. Biochem. Cell Biol.* **31,** 43–57
50. Silvera, D., Formenti, S. C., and Schneider, R. J. (2010) Translational control in cancer. *Nat. Rev. Cancer* **10,** 254–266
51. Ueda, T., Sasaki, M., Elia, A. J., Chio, I. I. C., Hamada, K., Fukunaga, R., and Mak, T. W. (2010) Combined deficiency for MAP kinase-interacting kinase 1 and 2 (Mnk1 and Mnk2) delays tumor development. *Proc. Natl. Acad. Sci. U.S.A.* **107,** 13984–13990
52. Matsumoto, F., Fujii, H., Abe, M., Kajino, K., Kobayashi, T., Matsumoto, T., Ikeda, K., and Hino, O. (2006) A novel tumor marker, Niban, is expressed in subsets of thyroid tumors and Hashimoto's thyroiditis. *Hum. Pathol.* **37,** 1592–1600
53. Kannangai, R., Diehl, A. M., Sicklick, J., Rojkind, M., Thomas, D., and Torbenson, M. (2005) Hepatic angiomyolipoma and hepatic stellate cells share a similar gene expression profile. *Hum. Pathol.* **36,** 341–347
54. Ito, S., Fujii, H., Matsumoto, T., Abe, M., Ikeda, K., and Hino, O. (2010) Frequent expression of Niban in head and neck squamous cell carcinoma and squamous dysplasia. *Head Neck* **32,** 96–103
55. Ji, H., Ding, Z., Hawke, D., Xing, D., Jiang, B.-H., Mills, G. B., and Lu, Z. (2012) AKT-dependent phosphorylation of Niban regulates nucleophosmin- and MDM2-mediated p53 stability and cell apoptosis. *EMBO Rep.* **13,** 554–560
56. Chen, S., Evans, H. G., and Evans, D. R. (2011) FAM129B/MINERVA, a novel adherens junction-associated protein, suppresses apoptosis in HeLa cells. *J. Biol. Chem.* **286,** 10201–10209
57. Old, W. M., Shabb, J. B., Houel, S., Wang, H., Couts, K. L., Yen, C., Litman, E. S., Croy, C. H., Meyer-Arendt, K., Miranda, J. G., Brown, R. A., Witze, E. S., Schweppe, R. E., Resing, K. A., and Ahn, N. G. (2009)

Functional proteomics identifies targets of phosphorylation by B-Raf signaling in melanoma. *Mol. Cell* **34,** 115–131
58. Hsu, P. P., Kang, S. A., Rameseder, J., Zhang, Y., Ottina, K. A., Lim, D., Peterson, T. R., Choi, Y., Gray, N. S., Yaffe, M. B., Marto, J. A., and Sabatini, D. M. (2011) The mTOR-regulated phosphoproteome reveals a mechanism of mTORC1-mediated inhibition of growth factor signaling. *Science* **332,** 1317–1322
59. Wang, L., Harris, T. E., and Lawrence, J. C. (2008) Regulation of Proline-rich Akt Substrate of 40 kDa (PRAS40) Function by Mammalian Target of Rapamycin Complex 1 (mTORC1)-mediated Phosphorylation. *J. Biol. Chem.* **283,** 15619–15627
60. Zenke, F. T., Krendel, M., DerMardirossian, C., King, C. C., Bohl, B. P., and Bokoch, G. M. (2004) p21-activated kinase 1 phosphorylates and regulates 14–3-3 binding to GEF-H1, a microtubule-localized Rho exchange factor. *J. Biol. Chem.* **279,** 18392–18400
61. Kissil, J. L., Wilker, E. W., Johnson, K. C., Eckman, M. S., Yaffe, M. B., and Jacks, T. (2003) Merlin, the product of the Nf2 tumor suppressor gene, is an inhibitor of the p21-activated kinase, Pak1. *Mol. Cell* **12,** 841–849
62. Kashatus, D. F. (2013) Ral GTPases in tumorigenesis: emerging from the shadows. *Exp. Cell Res.* **319,** 2337–2342
63. Tong, J., Taylor, P., Peterman, S. M., Prakash, A., and Moran, M. F. (2009) Epidermal growth factor receptor phosphorylation sites Ser991 and Tyr998 are implicated in the regulation of receptor endocytosis and phosphorylations at Ser1039 and Thr1041. *Mol. Cell. Proteomics MCP* **8,** 2131–2144
64. Assiddiq, B. F., Tan, K. Y., Toy, W., Chan, S. P., Chong, P. K., and Lim, Y. P. (2012) EGFR S1166 phosphorylation induced by a combination of EGF and Gefitinib has a potentially negative impact on lung cancer cell growth. *J. Proteome Res.* **11,** 4110–4119
65. Ying, H., Zheng, H., Scott, K., Wiedemeyer, R., Yan, H., Lim, C., Huang, J., Dhakal, S., Ivanova, E., Xiao, Y., Zhang, H., Hu, J., Stommel, J. M., Lee, M. A., Chen, A.-J., Paik, J.-H., Segatto, O., Brennan, C., Elferink, L. A., Wang, Y. A., Chin, L., and DePinho, R. A. (2010) Mig-6 controls EGFR trafficking and suppresses gliomagenesis. *Proc. Natl. Acad. Sci. U.S.A.* **107,** 6912–6917
66. Gioeli, D., Wunderlich, W., Sebolt-Leopold, J., Bekiranov, S., Wulfkuhle, J. D., Petricoin, E. F., Conaway, M., and Weber, M. J. (2011) Compensatory pathways induced by MEK inhibition are effective drug targets for combination therapy against castration-resistant prostate cancer. *Am. Assoc. Cancer Res.* **10,** 1581–1590
67. Fritsche, L., Neukamm, S. S., Lehmann, R., Kremmer, E., Hennige, A. M., Hunder-Gugel, A., Schenk, M., Häring, H.-U., Schleicher, E. D., and Weigert, C. (2011) Insulin-induced serine phosphorylation of IRS-2 via ERK1/2 and mTOR: studies on the function of Ser675 and Ser907. *Am. J. Physiol. - Endocrinol. Metab.* **300,** E824-E836
68. Nobusawa, S., Watanabe, T., Kleihues, P., and Ohgaki, H. (2009) IDH1 Mutations as molecular signature and predictive factor of secondary glioblastomas. *Clin. Cancer Res.* **15,** 6002–6007
69. Yang, H., Ye, D., Guan, K.-L., and Xiong, Y. (2012) IDH1 and IDH2 mutations in tumorigenesis: mechanistic insights and clinical perspectives. *Clin. Cancer Res.* **18,** 5562–5571
70. Lu, C., Ward, P. S., Kapoor, G. S., Rohle, D., Turcan, S., Abdel-Wahab, O., Edwards, C. R., Khanin, R., Figueroa, M. E., Melnick, A., Wellen, K. E., O'Rourke, D. M., Berger, S. L., Chan, T. A., Levine, R. L., Mellinghoff, I. K., and Thompson, C. B. (2012) IDH mutation impairs histone demethylation and results in a block to cell differentiation. *Nature* **483,** 474–478
71. Chantalat, S., Depaux, A., Héry, P., Barral, S., Thuret, J.-Y., Dimitrov, S., and Gérard, M. (2011) Histone H3 trimethylation at lysine 36 is associated with constitutive and facultative heterochromatin. *Genome Res.* **21,** 1426–1437
72. Bannister, A. J., Zegerman, P., Partridge, J. F., Miska, E. A., Thomas, J. O., Allshire, R. C., and Kouzarides, T. (2001) Selective recognition of methylated lysine 9 on histone H3 by the HP1 chromo domain. *Nature* **410,** 120–124
73. Wang, Z., Zang, C., Rosenfeld, J. A., Schones, D. E., Barski, A., Cuddapah, S., Cui, K., Roh, T.-Y., Peng, W., Zhang, M. Q., and Zhao, K. (2008) Combinatorial patterns of histone acetylations and methylations in the human genome. *Nat. Genet.* **40,** 897–903
74. Agalioti, T., Chen, G., and Thanos, D. (2002) Deciphering the transcriptional histone acetylation code for a human gene. *Cell* **111,** 381–392
75. Fujii, T., Khawaja, M. R., DiNardo, C. D., Atkins, J. T., and Janku, F. Targeting isocitrate dehydrogenase (IDH) in cancer. *Discov. Med.* 21, 373–380
76. Cui, D., Ren, J., Shi, J., Feng, L., Wang, K., Zeng, T., Jin, Y., and Gao, L. (2016) R132H mutation in IDH1 gene reduces proliferation, cell survival and invasion of human glioma by downregulating Wnt/β-catenin signaling. *Int. J. Biochem. Cell Biol.* **73,** 72–81
77. Kamino, M., Kishida, M., Kibe, T., Ikoma, K., Iijima, M., Hirano, H., Tokudome, M., Chen, L., Koriyama, C., Yamada, K., Arita, K., and Kishida, S. (2011) Wnt-5a signaling is correlated with infiltrative activity in human glioma by inducing cellular migration and MMP-2. *Cancer Sci.* **102,** 540–548
78. Shojima, K., Sato, A., Hanaki, H., Tsujimoto, I., Nakamura, M., Hattori, K., Sato, Y., Dohi, K., Hirata, M., Yamamoto, H., and Kikuchi, A. (2015) Wnt5a promotes cancer cell invasion and proliferation by receptor-mediated endocytosis-dependent and -independent mechanisms, respectively. *Sci. Rep.* **5,** 8042
79. Thiele, S., Göbel, A., Rachner, T. D., Fuessel, S., Froehner, M., Muders, M. H., Baretton, G. B., Bernhardt, R., Jakob, F., Glüer, C. C., Bornhäuser, M., Rauner, M., and Hofbauer, L. C. (2015) WNT5A has anti-prostate cancer effects in vitro and reduces tumor growth in the skeleton in vivo. *J. Bone Miner. Res.* **30,** 471–480
80. Jönsson, M., Dejmek, J., Bendahl, P.-O., and Andersson, T. (2002) Loss of Wnt-5a protein is associated with early relapse in invasive ductal breast carcinomas. *Cancer Res.* **62,** 409–416
81. Zhang, Y., Du, J., Zheng, J., Liu, J., Xu, R., Shen, T., Zhu, Y., Chang, J., Wang, H., Zhang, Z., Meng, F., Wang, Y., Chen, Y., Xu, Y., and Gu, L. (2015) EGF-reduced Wnt5a transcription induces epithelial-mesenchymal transition via Arf6-ERK signaling in gastric cancer cells. *Oncotarget* **6,** 7244–7261
82. Kitai, R., Horita, R., Sato, K., Yoshida, K., Arishima, H., Higashino, Y., Hashimoto, N., Takeuchi, H., Kubota, T., and Kikuta, K.-I. (2010) Nestin expression in astrocytic tumors delineates tumor infiltration. *Brain Tumor Pathol.* **27,** 17–21
83. Lu, W. J., Lan, F., He, Q., Lee, A., Tang, C. Z., Dong, L., Lan, B., Ma, X., Wu, J. C., and Shen, L. (2011) Inducible expression of stem cell associated intermediate filament nestin reveals an important role in glioblastoma carcinogenesis. *Int. J. Cancer J. Int. Cancer* **128,** 343–351
84. Forbes, S. A., Bhamra, G., Bamford, S., Dawson, E., Kok, C., Clements, J., Menzies, A., Teague, J. W., Futreal, P. A., and Stratton, M. R. (2008) The Catalogue of Somatic Mutations in Cancer (COSMIC). *Curr. Protoc. Hum. Genet. Genet. Editor. Board Jonathan Haines Al* CHAPTER, Unit–10.11
85. Hirokawa, Y., Tikoo, A., Huynh, J., Utermark, T., Hanemann, C. O., Giovannini, M., Xiao, G.-H., Testa, J. R., Wood, J., and Maruta, H. (2004) A clue to the therapy of neurofibromatosis type 2: NF2/merlin is a PAK1 inhibitor. *Cancer J. Sudbury Mass* **10,** 20–26
86. Trovó-Marqui, A., and Tajara, E. (2006) Neurofibromin: a general outlook. *Clin. Genet.* **70,** 1–13
87. Johnson, M. R., DeClue, J. E., Felzmann, S., Vass, W. C., Xu, G., White, R., and Lowy, D. R. (1994) Neurofibromin can inhibit Ras-dependent growth by a mechanism independent of its GTPase-accelerating function. *Mol. Cell. Biol.* **14,** 641–645
88. Gutmann, D. H. (2001) The neurofibromatoses: when less is more. *Hum. Mol. Genet.* **10,** 747–755
89. Lau, N., Feldkamp, M. M., Roncari, L., Loehr, A. H., Shannon, P., Gutmann, D. H., and Guha, A. (2000) Loss of neurofibromin is associated with activation of RAS/MAPK and PI3-K/AKT signaling in a neurofibromatosis 1 astrocytoma. *J. Neuropathol. Exp. Neurol.* **59,** 759–767
90. Petrilli, A. M., and Fernández-Valle, C. (2015) Role of Merlin/NF2 inactivation in tumor biology. *Oncogene*,
91. Britten, C. D. (2013) PI3K and MEK inhibitor combinations: examining the evidence in selected tumor types. *Cancer Chemother. Pharmacol.* **71,** 1395–1409
92. Aoki, H., Yokoyama, T., Fujiwara, K., Tari, A. M., Sawaya, R., Suki, D., Hess, K. R., Aldape, K. D., Kondo, S., Kumar, R., and Kondo, Y. (2007) Phosphorylated Pak1 level in the cytoplasm correlates with shorter survival time in patients with glioblastoma. *Clin. Cancer Res.* **13,** 6603–6609
93. Kumar, R., Gururaj, A. E., and Barnes, C. J. (2006) p21-activated kinases in cancer. *Nat. Rev. Cancer* **6,** 459–471

94. Kesanakurti, D., Chetty, C., Rajasekhar Maddirela, D., Gujrati, M., and Rao, J. S. (2012) Functional cooperativity by direct interaction between PAK4 and MMP-2 in the regulation of anoikis resistance, migration and invasion in glioma. *Cell Death Dis.* **3,** e445
95. Di, J., Huang, H., Qu, D., Tang, J., Cao, W., Lu, Z., Cheng, Q., Yang, J., Bai, J., Zhang, Y., and Zheng, J. (2015) Rap2B promotes proliferation, migration, and invasion of human breast cancer through calcium-related ERK1/2 signaling pathway. *Sci. Rep.* 5
96. Gutierrez-Erlandsson, S., Herrero-Vidal, P., Fernandez-Alfara, M., Hernandez-Garcia, S., Gonzalo-Flores, S., Mudarra-Rubio, A., Fresno, M., and Cubelos, B. (2013) R-RAS2 overexpression in tumors of the human central nervous system. *Mol. Cancer* **12,** 127
97. Loilome, W., Joshi, A. D., Rhys C. M. J. ap, Piccirillo, S., Angelo, V. L., Gallia, G. L., and Riggins, G. J. (2009) Glioblastoma cell growth is suppressed by disruption of fibroblast growth factor pathway signaling. *J. Neurooncol.* **94,** 359–366
98. Miao, H., Gale, N. W., Guo, H., Qian, J., Petty, A., Kaspar, J., Murphy, A. J., Valenzuela, D. M., Yancopoulos, G., Hambardzumyan, D., Lathia, J. D., Rich, J. N., Lee, J., and Wang, B. (2015) EphA2 promotes infiltrative invasion of glioma stem cells in vivo through crosstalk with Akt and regulates stem properties. *Oncogene* **34,** 558–567
99. Day, B. W., Stringer, B. W., and Boyd, A. W. (2014) Eph receptors as therapeutic targets in glioblastoma. *Br. J. Cancer* **111,** 1255–1261
100. Lee, P., Murphy, B., Miller, R., Menon, V., Banik, N. L., Giglio, P., Lindhorst, S. M., Varma, A. K., Vandergrift, W. A., Patel, S. J., and Das, A. (2015) Mechanisms and clinical significance of histone deacetylase inhibitors: epigenetic glioblastoma therapy. *Anticancer Res.* **35,** 615–625
101. Chen, Y., Sprung, R., Tang, Y., Ball, H., Sangras, B., Kim, S. C., Falck, J. R., Peng, J., Gu, W., and Zhao, Y. (2007) Lysine propionylation and butyrylation are novel post-translational modifications in histones. *Mol. Cell. Proteomics* **6,** 812–819
102. Vogelauer, M., Krall, A. S., McBrian, M. A., Li, J.-Y., and Kurdistani, S. K. (2012) Stimulation of histone deacetylase activity by metabolites of intermediary metabolism. *J. Biol. Chem.* **287,** 32006–32016
103. Eliuk, S. M., Maltby, D., Panning, B., and Burlingame, A. L. (2010) High resolution electron transfer dissociation studies of unfractionated intact histones from murine embryonic stem cells using on-line capillary LC separation. *Mol. Cell. Proteomics MCP* **9,** 824–837
104. Young, N. L., DiMaggio, P. A., Plazas-Mayorca, M. D., Baliban, R. C., Floudas, C. A., and Garcia, B. A. (2009) High throughput characterization of combinatorial histone codes. *Mol. Cell. Proteomics* **8,** 2266–2284